JOURNAL OF COMPUTATIONAL PHYSICS 81, 1–52 (1989)

Review Article

An Analysis of Finite-Difference and Finite-Volume Formulations of Conservation Laws*

MARCEL VINOKUR

Sterling Software, Palo Alto, California 94303

Received January 5, 1988; revised June 6, 1988

Finite-difference and finite-volume formulations are analyzed in order to clear up the confusion concerning their application to the numerical solution of conservation laws. A new coordinate-free formulation of systems of conservation laws is developed, which clearly distinguishes the role of physical vectors from that of algebraic vectors which characterize the system. The analysis considers general types of equations—potential, Euler, and Navier–Stokes. Three-dimensional unsteady flows with time-varying grids are described using a single, consistent nomenclature for both formulations. Grid motion due to a non-inertial reference frame as well as flow adaptation is covered. In comparing the two formulations, it is found useful to distinguish between differences in numerical methods and differences in grid definition. The former plays a role for non-Cartesian grids and results in only cosmetic differences in the manner in which geometric terms are handled. The differences in grid definition for the two formulations is found to be more important, since it affects the manner in which boundary conditions, zonal procedures, and grid singularities are handled at computational boundaries. The proper interpretation of strong and weak conservation-law forms for quasi-one-dimensional and axisymmetric flows is brought out.

INTRODUCTION

Many current algorithms in computational fluid dynamics are based on the numerical solution of conservation laws. This choice is motivated by several considerations, the chief one being the ability to treat flow discontinuities automatically. In an earlier paper [1] the author treated the differential formulation of the conservation equations. This formulation forms the basis for finite-difference algorithms, which are historically very old. The more fundamental integral formulation is the basis for finite-volume algorithms. These appeared more recently (probably the earliest is found in [2]) and are not as well known. There appears to be some confusion and ignorance concerning the relation of these two approaches. The primary purpose of this paper is to shed some light on this subject. For this purpose, it is useful to distinguish between the method of approach (integral vs

* This research was supported by NASA Ames Research Center under Contracts NCC 2-16 and NAS 2-11555.

0021-9991/89 $3.00

differential) and grid definition (grid points represent vertices or centers of cells). It turns out that the differences in method only play a role for non-Cartesian grids and manifest themselves in the manner in which the geometry of the grid is handled. The effect on the numerical results is generally small in most cases. The differences in grid definition are important at computational boundaries, where they determine the manner in which boundary conditions, zonal procedures, and grid singularities are handled.

To provide the greatest possible utility, a unified presentation covering all classes of equations is given. Both approaches are described using a well-defined, consistent nomenclature. This is accomplished by employing geometric concepts which lead to an unorthodox treatment of the differential formulation. Thus, when dealing with coordinate transformations, terms such as volumes, areas, and normal velocity components are used instead of Jacobians, metrics, and contravariant velocity components. The general case of 3-dimensional unsteady flow with time-varying grids is considered and specialized to other cases when necessary. Only those aspects of algorithms that relate to the comparison of the two approaches are presented.

In order to make the discussion more physical and compact, vector notation is used throughout. Here the word vector refers to physical vectors (e.g., velocity or momentum) as distinguished from algebraic *vectors* (e.g., the set of conservative variables). It is customary to replace the vector momentum equation by its scalar components, so that only algebraic *vectors* and matrices are encountered. To allow for arbitrary scalar decompositions and to preserve the compactness, the momentum equation is here treated as a single vector equation. This necessitates the introduction of a novel treatment of flux *vectors* and flux Jacobian matrices solely in terms of physical vectors and independent of a coordinate system.

The integral formulation of general conservation laws is presented first and is then used to derive the differential formulation. The new vector formulation of flux Jacobian matrices follows, with applications to Roe averaging and flux-vector splitting. The next section presents the discretization of the equations, beginning with a careful discussion of grid definition. The general characteristics of standard finite-difference methods are described, and some of the inaccuracies arising from the treatment of the grid geometry are enumerated. The discussion of finite-volume methods first details various geometric constructions, including a unified presentation of different methods to calculate the cell volume. The three main types of equations–Euler, Navier–Stokes, and potential are each discussed in turn, and specific comparisons of the two approaches are made. Both centered and upwind treatments of inviscid flux terms are considered. The section on moving grids presents in a unified way the combined effects of a non-inertial reference frame and grid motion with respect to that frame due to flow adaptation. The role of the two types of grids in formulating wall boundary conditions, zonal boundaries, and grid singularities is covered in the next section. The following section discusses strong and weak conservation-law forms and their relation to quasi-one-dimensional and axisymmetric flow. The concluding section contains brief discussions of hybrid methods and the relation of finite-element and finite-volume methods.

FORMULATION OF CONSERVATION LAWS

Integral Formulation

Let the position vector $\mathbf{r}$ of a point in space and time t be defined with respect to an inertial reference frame. Since physical conservation only has meaning over a finite region of space and a finite interval of time, we divide the flow region into contiguous cells which can vary with time. The general form of a conservation law for a given cell is

$$\int_{V(t_2)} U\,dV - \int_{V(t_1)} U\,dV + \int_{t_1}^{t_2} \oint_{S(t)} \mathbf{n}\cdot\mathbf{F}\,dS\,dt = \int_{t_1}^{t_2} \int_{V(t)} P\,dV\,dt, \tag{1}$$

where $V(t)$ is the cell volume, $\mathbf{n}\,dS(t)$ is a vector element of surface area with outward normal $\mathbf{n}$, U is a conservative variable per unit volume, $\mathbf{F}$ is the flux of U per unit area per unit time, and P is the rate of production of U per unit volume per unit time. If U and P are scalars, then $\mathbf{F}$ is a vector; while if U and P are vectors, $\mathbf{F}$ is a tensor. An example of P is the rate of production of a chemical species. Let $\mathbf{u}$ and $\mathbf{v}(t)$ be the fluid velocity and surface element velocity, respectively. The flux $\mathbf{F}$ can then be written as

$$\mathbf{F} = (\mathbf{u} - \mathbf{v})\,U + \mathbf{G}, \tag{2}$$

where the first term is the convection of U relative to the surface element, and $\mathbf{G}$ stands for the non-convective part of the flux. It is often convenient to define the cell geometry with respect to a non-inertial reference frame. In this case, let $\mathbf{r}_0(t)$, $\mathbf{v}_0(t)$, and $\boldsymbol{\Omega}(t)$ be the position vector of the origin, velocity, and angular velocity of the non-inertial frame relative to the inertial frame. Then $\mathbf{v}$ can be written as

$$\mathbf{v} = \mathbf{v}_r + \mathbf{v}_c, \tag{3}$$

where

$$\mathbf{v}_r = \mathbf{v}_0(t) + \boldsymbol{\Omega}(t) \times [\mathbf{r} - \mathbf{r}_0(t)], \tag{4}$$

and $\mathbf{v}_c(t)$ is the surface element velocity relative to the non-inertial frame, but expressed in the inertial frame. The velocity $\mathbf{v}_c$ can be determined by the motion of a well-defined surface, or some flow gradients (adaptive grid). The case $\mathbf{u} = \mathbf{v}$ corresponds to a Lagrangian cell.

The state of the fluid is specified in terms of a primary or primitive variable Q. An example of a flow governed by a single conservation law is potential flow, for which Q is the velocity potential ϕ and U is the density ρ. In general the flow is governed by a system of conservation laws, in which case U, $\mathbf{F}$, P, and Q represent

a set of variables. The primitive variables Q for the conservation of mass, momentum, and energy are ρ, $\mathbf{u}$, and the specific internal energy ε. The corresponding conservative variables U are ρ, the momentum per unit volume $\mathbf{m}=\rho\mathbf{u}$, and the total energy per unit volume $e=\rho(\varepsilon+\frac{1}{2}\mathbf{u}\cdot\mathbf{u})$. For nonequilibrium flow, the partial density of various species and the energy of internal states of species can be additional variables. In some turbulence models, additional variables for turbulent quantities may be required. In order to close the system of equations one needs an equation of state and possibly additional relations to define transport coefficients and the production terms P.

For the Euler equations, both $\mathbf{F}$ and U are functions of Q, and consequently $\mathbf{F}$ can be expressed as a function of U. For the Navier–Stokes equations, $\mathbf{F}$ depends additionally on ∇Q, where the notation ∇Q denotes the gradient of Q, its transpose, or the divergence of Q. (If thermal radiation is present, $\mathbf{F}$ can involve integrals of Q, and additional integro-differential equations would be required. This case is not discussed in this paper.) For potential flow, both $\mathbf{F}$ and U also depend on ∇Q as well as $\partial Q/\partial t$ in the unsteady case. For all flows, an additional explicit dependence on $\mathbf{r}$ and t comes from the surface element velocity $\mathbf{v}$. We thus note that the integral formulation may require spatial and temporal derivatives of Q to be calculated.

If we assume all variables are continuous in time, then Eq. (1) reduces to

$$\frac{d}{dt}\int_V U\,dV+\oint_S \mathbf{n}\cdot\mathbf{F}\,dS=\int_V P\,dV. \tag{5}$$

This is the usual statement of a conservation law. For steady-flow calculations, the first term is absent. Even when it is employed in time asymptotic marching techniques, it need not be treated accurately. This poses less stringent conditions on the numerical algorithm. In many applications, Eq. (5) is only satisfied in a global sense, over the complete flow region. In this sense it is used as an overall check on a numerical method. There are additional global conservation laws that can be derived under special assumptions that are sometimes used as constraints in an algorithm. Examples are conservation of entropy (inviscid, continuous flows), kinetic energy (incompressible, inviscid flow), and vorticity (plane incompressible flow). In this paper only local conservation laws that serve to define the basic numerical method will be considered.

Certain geometric identities can be derived as special cases of Eq. (1). The condition that the cell is closed is given by

$$\oint_S \mathbf{n}\,dS=0. \tag{6}$$

The relative rigid body motion of two frames of reference is expressed by

$$\oint_S \mathbf{n}\cdot\mathbf{v}_r\,dS=0. \tag{7}$$

Using Eqs. (4) and (6), this can be replaced by

$$\oint_S \mathbf{r} \times \mathbf{n}\, dS = 0. \tag{8}$$

The conservation of volume for a time-varying cell is given by

$$V(t_2) - V(t_1) = \int_{t_1}^{t_2} \oint_{S(t)} \mathbf{n} \cdot \mathbf{v}_c\, dS\, dt. \tag{9}$$

An additional geometric constraint is that the sum of the cell volumes must equal the total volume of the flow region.

A main motivation for the conservative formulation is to capture flow discontinuities in inviscid flow. The jump conditions across such discontinuities are just limiting forms of the integral relations. Applying Eq. (5) to a pill box with faces ΔS_1 and ΔS_2 straddling a surface of discontinuity whose normal in a positive direction is $\mathbf{n}$, we obtain in the limit the jump conditions

$$\int_{\Delta S_1} \mathbf{n} \cdot \mathbf{F}\, dS = \int_{\Delta S_2} \mathbf{n} \cdot \mathbf{F}\, dS. \tag{10}$$

Actually, since the geometry of space is continuous, Eq. (10) can be replaced by the weaker relation

$$\mathbf{n} \cdot (\mathbf{F}_1 - \mathbf{F}_2) = 0. \tag{11}$$

It is possible for algorithms to satisfy the weak form of the jump conditions and violate strict conservation.

Differential Formulation

The differential formulation is obtained by applying Eq. (5) to a differential cell in physical space which is the image of the computational cell $d\xi\, d\eta\, d\zeta$ resulting from the coordinate transformation

$$\begin{aligned} \mathbf{r} &= \mathbf{r}(\xi, \eta, \zeta, \tau) \\ t &= \tau. \end{aligned} \tag{12}$$

Let $\mathbf{S}^\xi\, d\eta\, d\zeta$ be the surface area vector in the positive ξ direction (with analogous definitions for the other directions), and $V\, d\xi\, d\eta\, d\zeta$ be the volume of the differential cell. Equation (5) then takes the form

$$(UV)_\tau + (\mathbf{S}^\xi \cdot \mathbf{F})_\xi + (\mathbf{S}^\eta \cdot \mathbf{F})_\eta + (\mathbf{S}^\zeta \cdot \mathbf{F})_\zeta = PV, \tag{13}$$

where subscripts indicate partial differentiation,

$$\begin{aligned} \mathbf{S}^{\xi} &= \mathbf{r}_{\eta} \times \mathbf{r}_{\zeta} \\ \mathbf{S}^{\eta} &= \mathbf{r}_{\zeta} \times \mathbf{r}_{\xi} \\ \mathbf{S}^{\zeta} &= \mathbf{r}_{\xi} \times \mathbf{r}_{\eta}, \end{aligned} \tag{14}$$

and

$$V = \mathbf{r}_{\xi} \cdot \mathbf{r}_{\eta} \times \mathbf{r}_{\zeta}. \tag{15}$$

The quantity V is also equal to the Jacobian J or J^{-1} of the coordinate transformation.

In expressing U, $\mathbf{F}$, and P as functions of Q and its derivatives, the relations

$$\mathbf{v} = \mathbf{r}_{\tau}, \tag{16}$$

$$\nabla Q = \nabla \xi Q_{\xi} + \nabla \eta Q_{\eta} + \nabla \zeta Q_{\zeta} \tag{17}$$

are used, where

$$\nabla \xi = \mathbf{S}^{\xi}/V, \qquad \nabla \eta = \mathbf{S}^{\eta}/V, \qquad \nabla \zeta = \mathbf{S}^{\zeta}/V, \tag{18}$$

and

$$\partial Q/\partial t = Q_{\tau} - \mathbf{r}_{\tau} \cdot \nabla Q. \tag{19}$$

From Eq. (19) one can obtain the relations $\partial \xi/\partial t = -\mathbf{r}_{\tau} \cdot \nabla \xi$, etc., for the time derivatives of the inverse transformation. Equation (13) can also be written in the equivalent "Cartesian" form

$$\hat{U}_{\tau} + (\hat{F}^{\xi})_{\xi} + (\hat{F}^{\eta})_{\eta} + (\hat{F}^{\zeta})_{\zeta} = \hat{P}, \tag{20}$$

where

$$\hat{U} = UV, \qquad \hat{F}^{\xi} = \mathbf{S}^{\xi} \cdot \mathbf{F}, \qquad \hat{F}^{\eta} = \mathbf{S}^{\eta} \cdot \mathbf{F}, \qquad \hat{F}^{\zeta} = \mathbf{S}^{\zeta} \cdot \mathbf{F}, \qquad \hat{P} = PV.$$

The geometric identities (6) and (9) become

$$(\mathbf{S}^{\xi})_{\xi} + (\mathbf{S}^{\eta})_{\eta} + (\mathbf{S}^{\zeta})_{\zeta} = 0 \tag{21}$$

and

$$V_{\tau} = (\mathbf{S}^{\xi} \cdot \mathbf{r}_{\tau})_{\xi} + (\mathbf{S}^{\eta} \cdot \mathbf{r}_{\tau})_{\eta} + (\mathbf{S}^{\zeta} \cdot \mathbf{r}_{\tau})_{\zeta}. \tag{22}$$

Equation (22) is called the differential statement of the geometric conservation law in [3]. Using Eqs. (21) and (22), Eq. (13) can also be written in the quasi-conservative form

$$U_{\tau} + \nabla \xi \cdot (\mathbf{F}'_{\xi} - \mathbf{r}_{\tau} U_{\xi}) + \nabla \eta \cdot (\mathbf{F}'_{\eta} - \mathbf{r}_{\tau} U_{\eta}) + \nabla \zeta \cdot (\mathbf{F}'_{\zeta} - \mathbf{r}_{\tau} U_{\zeta}) = P, \tag{23}$$

where

$$\mathbf{F}' = \mathbf{u}U + \mathbf{G}.$$

The above form is called the chain rule conservation law form in [4].

New Coordinate-Free Treatment of Flux Vectors

We have seen that Eq. (1) can represent a scalar or vector conservation law. Here the word vector refers to a physical vector such as position, velocity, or momentum and is represented by a bold faced symbol or an arrow. The related higher order quantity is a tensor. It is also convenient to express a set of variables as an algebraic *vector* and represent it as a column or a row. The related higher order quantity is a matrix. Since all calculations must ultimately be done with numbers, and to avoid the confusion between the two uses of the term vector, the momentum conservation law is normally treated as three scalar laws for the components of the momentum. A compactness and greater physical insight can be obtained by retaining the physical vectors as components of the algebraic *vectors*. The procedure will be illustrated for the inviscid flow of a perfect gas.

Vector Formulation of Flux Jacobian Matrices

The set of conservative variables U is given by the column *vector*

$$U = \begin{bmatrix} \rho \\ \mathbf{m} \\ e \end{bmatrix}. \tag{24}$$

Let $\mathbf{n}$ be the normal in a positive direction to a cell surface or a coordinate surface. One can then define the normal flux component $F_n = \mathbf{n} \cdot \mathbf{F}$, the normal velocity components $u_n = \mathbf{n} \cdot \mathbf{u}$ and $v_n = \mathbf{n} \cdot \mathbf{v}$, and the normal relative velocity component $u' = \mathbf{n} \cdot (\mathbf{u} - \mathbf{v}) = u_n - v_n$. For inviscid flow, the set of variables F_n is given by the column *vector*

$$F_n = \begin{bmatrix} M \\ \mathbf{P} \\ E \end{bmatrix} = \begin{bmatrix} \rho u' \\ \mathbf{m}u' + p\mathbf{n} \\ eu' + pu_n \end{bmatrix}, \tag{25}$$

where M, $\mathbf{P}$, and E are the normal flux of mass, momentum, and energy, and p is the pressure.

The *vector* F_n is a non-linear function of the *vector* U. In many algorithms one therefore employs a linearization in time or space. This requires the calculation of

dF_n in terms of dU. If v_n and $\mathbf{n}$ are held fixed, the first component of dF_n can be written as

$$d(\rho u') = -v_n\, d\rho + \mathbf{n} \cdot d\mathbf{m}. \tag{26}$$

This can be rewritten in the form of a matrix multiplication as

$$d(\rho u') = [-v_n\, \mathbf{n}\, 0] \begin{bmatrix} d\rho \\ d\mathbf{m} \\ de \end{bmatrix}, \tag{27}$$

where the dot product is implied in multiplying the second element of the row *vector* by the second element of the column *vector*. Applying the same procedure to the other components of dF_n, we can define a flux Jacobian matrix operator A satisfying $dF_n = A\, dU$, using the convention that in forming the product of a matrix element with a *vector* element, a dot product is implied if each element is either a physical vector or a tensor. For a perfect gas satisfying the equation of state

$$p = \kappa\rho\varepsilon, \qquad \kappa = \gamma - 1, \tag{28}$$

the matrix A can then be written as

$$A = \begin{bmatrix} -v_n & \mathbf{n} & 0 \\ \kappa b_1 \mathbf{n} - u_n \mathbf{u} & \mathbf{u}\mathbf{n} - \kappa \mathbf{n}\mathbf{u} + u'\mathbf{I} & \kappa \mathbf{n} \\ (\kappa b_1 - H)\, u_n & H\mathbf{n} - \kappa u_n \mathbf{u} & u' + \kappa u_n \end{bmatrix}, \tag{29}$$

where $H = \gamma\varepsilon + \frac{1}{2}\mathbf{u} \cdot \mathbf{u}$ is the total enthalpy per unit mass, $b_1 = \frac{1}{2}\mathbf{u} \cdot \mathbf{u}$, and $\mathbf{I}$ is the identity tensor.

For some algorithms, one requires the diagonalization of A in the form $R^{-1}AR = \Lambda$, where Λ is the eigenvalue matrix, and R and R^{-1} are the right and left eigenvector matrices, respectively. For multiple space dimensions one requires a set of linearly independent eigenvectors corresponding to a repeated eigenvalue. Let $\mathbf{a}_i$ be an arbitrary set of spatial basis vectors, and $\mathbf{a}^j$ be the set of reciprocal basis vectors satisfying $\mathbf{a}_i \cdot \mathbf{a}^j = \delta_i^j$, where δ_i^j is the Kronecker delta. One can then define $a_{ni} = \mathbf{n} \cdot \mathbf{a}_i$, $\mathbf{b}_i = \mathbf{n} \times \mathbf{a}_i$, $a_n^j = \mathbf{n} \cdot \mathbf{a}^j$, and $\mathbf{b}^j = \mathbf{n} \times \mathbf{a}^j$. If β is an arbitrary scalar, the three matrices can be written in the most general form as

$$\Lambda = \begin{bmatrix} \lambda_1 \delta_i^j & 0 & 0 \\ 0 & \lambda_2 & 0 \\ 0 & 0 & \lambda_3 \end{bmatrix} = \begin{bmatrix} u'\delta_i^j & 0 & 0 \\ 0 & u' + c & 0 \\ 0 & 0 & u' - c \end{bmatrix}, \tag{30}$$

$$R = \begin{bmatrix} a_{ni} & 1 & 1 \\ a_{ni}\mathbf{u} + \beta \mathbf{b}_i & \mathbf{u} + c\mathbf{n} & \mathbf{u} - c\mathbf{n} \\ a_{ni} b_1 + \beta \mathbf{b}_i \cdot \mathbf{u} & H + c u_n & H - c u_n \end{bmatrix}, \tag{31}$$

and

$$R^{-1}=\begin{bmatrix} a_n^j(1-b_3)-\beta^{-1}(\mathbf{b}^j\cdot\mathbf{u}) & a_n^j b_2\mathbf{u}+\beta^{-1}\mathbf{b}^j & -a_n^j b_2 \\ \tfrac{1}{2}(b_3-u_n/c) & -\tfrac{1}{2}(b_2\mathbf{u}-\mathbf{n}/c) & \tfrac{1}{2}b_2 \\ \tfrac{1}{2}(b_3+u_n/c) & -\tfrac{1}{2}(b_2\mathbf{u}+\mathbf{n}/c) & \tfrac{1}{2}b_2 \end{bmatrix}, \tag{32}$$

where $c=(\gamma p/\rho)^{1/2}$ is the speed of sound, $b_2=\kappa/c^2$, and $b_3=b_2b_1$. For three dimensions, A is a five by five matrix, while R has five columns and R^{-1} has five rows. Since the basis vectors $\mathbf{a}_i$ are linearly independent, it follows that the three eigenvectors corresponding to the repeated eigenvalue λ_1 are linearly independent. A useful choice for the basis vectors is to let one of the $\mathbf{a}_i$ be parallel to $\mathbf{n}$, so that the corresponding $\mathbf{b}_i=0$. The remaining $\mathbf{a}_i$ are then chosen to lie in the plane perpendicular to $\mathbf{n}$, so that their corresponding $a_{ni}=0$. Note that specific normalizations have been chosen for all the eigenvectors. Other normalizations may also be found useful.

One can define functions of the matrix A through

$$f(A)=f(\lambda_1)\,P_1+f(\lambda_2)\,P_2+f(\lambda_3)\,P_3, \tag{33}$$

where the projection operators P_1, P_2, and P_3 are matrices satisfying

$$R^{-1}P_1R=\begin{bmatrix}\delta_i^j & 0 & 0\\ 0 & 0 & 0\\ 0 & 0 & 0\end{bmatrix},\qquad R^{-1}P_2R=\begin{bmatrix}0 & 0 & 0\\ 0 & 1 & 0\\ 0 & 0 & 0\end{bmatrix},$$

$$R^{-1}P_3R=\begin{bmatrix}0 & 0 & 0\\ 0 & 0 & 0\\ 0 & 0 & 1\end{bmatrix}. \tag{34}$$

Examples of $f(\lambda)$ are λ, $|\lambda|$, $\operatorname{sgn}\lambda=|\lambda|/\lambda$, and $\lambda^{\pm}=(\lambda\pm|\lambda|)/2$. The formula for P_1 is

$$P_1=\begin{bmatrix}1-b_3 & b_2\mathbf{u} & -b_2\\ u_2\mathbf{n}-b_3\mathbf{u} & b_2\mathbf{u}\mathbf{u}-\mathbf{n}\mathbf{n}+\mathbf{I} & -b_2\mathbf{u}\\ u_n^2-(1+b_3)\,b_1 & (1+b_3)\mathbf{u}-u_n\mathbf{n} & -b_3\end{bmatrix}. \tag{35}$$

Using the fact that

$$P_1+P_2+P_3=I=\begin{bmatrix}1 & 0 & 0\\ 0 & \mathbf{I} & 0\\ 0 & 0 & 1\end{bmatrix}, \tag{36}$$

where I is the unit matrix, one can express the other two projection matrices as

$$P_{\substack{2\\3}}=\tfrac{1}{2}[\pm A/c+I(1\mp u'/c)-P_1]. \tag{37}$$

All the results obtained so far can be generalized to an arbitrary gas law.

In closing, one should note that the structures of matrices R and R^{-1} are different from those of A, P_1, P_2, and P_3, and the dot product convention may not necessarily apply to the first two. Actually, the convention is valid when forming the product of R^{-1} and a column *vector*. As an example, the product $R^{-1}R$ gives the identity matrix. On the other hand, in forming the product RR^{-1}, a tensor product is implied if each element is a vector. The result is the unit matrix I.

Roe Averaging

A large class of upwind-biased numerical approximations to the inviscid flux *vector* F_n, to be discussed in the next section, makes use of the properties of the matrix A. In a particular subclass, based on a local spatial linearization, A must be evaluated at some average of two neighboring states. Roe [5] suggested a specific average which gives the exact difference in flux if the two states correspond to a discontinuity. Thus, given two states U_L and U_R associated with the common surface vectors $\mathbf{n}$ and $\mathbf{v}$, the Roe averaged state $\bar{U}$ is defined by

$$F_n(U_R) - F_n(U_L) = A(\bar{U})(U_R - U_L). \tag{38}$$

The notation $\bar{U}$ implies only those variables that appear explicitly in A. A unique state $\bar{U}$ can be obtained by noting that the average velocity $\bar{\mathbf{u}}$ must be some linear combination of $\mathbf{u}_L$, $\mathbf{u}_R$, and $\mathbf{n}$. Upon substituting Eqs. (24), (25), and (29), and recalling that $\mathbf{u}_L$, $\mathbf{u}_R$, and $\mathbf{n}$ are arbitrary, independent vectors, one obtains from the second component of Eq. (38)

$$\bar{\mathbf{u}} = \alpha \mathbf{u}_L + (1-\alpha)\,\mathbf{u}_R, \tag{39}$$

where

$$\alpha = \sqrt{\rho_L}/(\sqrt{\rho_L} + \sqrt{\rho_R}). \tag{40}$$

Similarly, the third component of Eq. (38) then yields

$$\bar{H} = \alpha H_L + (1-\alpha)\,H_R. \tag{41}$$

The sound speed, derived from the total enthalpy via $c^2 = \kappa(H - \frac{1}{2}\mathbf{u}\cdot\mathbf{u})$, can be written as

$$\bar{c}^2 = \tfrac{1}{2}\kappa\alpha(1-\alpha)(\mathbf{u}_R - \mathbf{u}_L)\cdot(\mathbf{u}_R - \mathbf{u}_L) + \alpha c_L^2 + (1-\alpha)\,c_R^2. \tag{42}$$

The above derivation is much more direct than that found in [5]. One notes from Eq. (42) that $\bar{c}^2$ is greater than the weighted average of c_L^2 and c_R^2. It follows from Eq. (30) that for either λ_2 or λ_3, it is possible that the Roe-averaged eigenvalue could lie outside the range determined by the two states L and R. In particular, if the normal relative speed is very close to sonic for both states, the corresponding eigenvalues could both be of one sign, while the Roe-averaged

eigenvalue could have the opposite sign. Some numerical examples illustrating these phenomena are found in the Appendix. The implications for algorithms based on Roe's scheme should be studied further.

Flux-Vector Splitting

Another subclass of upwind-biased numerical approximations to the inviscid flux *vector* F_n is based on the eigenvalues of A. One notes from Eq. (30) that if $|u'| \geqslant c$, all the eigenvalues of A are of one sign, which determines the direction of the upwinding. For $|u'| < c$, the eigenvalues of A are of mixed sign. In flux-vector splitting methods the flux *vector* F_n is split into several parts, each of which has an unambiguous direction of upwinding determined by the signs of appropriate eigenvalues. The earliest methods utilize the homogeneity property

$$F_n = AU \tag{43}$$

valid for a gas satisfying

$$p = \rho f(\varepsilon). \tag{44}$$

(It is thus valid for a gas that is thermally perfect, but calorically imperfect.) Using Eqs. (33) and (43), one can split F_n as

$$F_n = F_{n1} + F_{n2} + F_{n3}, \tag{45}$$

where

$$F_{ni} = \lambda_i P_i U. \tag{46}$$

For a perfect gas one obtains

$$F_{n1} = \frac{\lambda_1 \rho \kappa}{\gamma} \begin{bmatrix} 1 \\ \mathbf{u} \\ \frac{1}{2}\mathbf{u}\cdot\mathbf{u} \end{bmatrix}, \qquad F_{\substack{n2 \\ 3}} = \frac{\lambda_2 \rho}{2\gamma} \begin{bmatrix} 1 \\ \mathbf{u} \pm c\mathbf{n} \\ H \pm cu_n \end{bmatrix}. \tag{47}$$

This form of flux splitting was first given in [6]. The earlier Steger and Warming splitting [7] is of the form

$$F_n = F_n^+ + F_n^-, \tag{48}$$

where the forward and backward flux *vectors* F_n^+ and F_n^- are obtained from Eq. (45) by substituting λ_i^+ and λ_i^-, respectively. If the normal relative speed is sonic or supersonic, one obtains

$$\begin{aligned} F_n^+ &= F_n, \quad F_n^- = 0 \quad \text{for } u' \geqslant c \\ F_n^- &= F_n, \quad F_n^+ = 0 \quad \text{for } u' \leqslant -c. \end{aligned} \tag{49}$$

One can show that all the eigenvalues of the split flux Jacobian matrices have the correct sign in the subsonic region for $\gamma < \frac{5}{3}$.

The above split fluxes are not continuously differentiable at the zeros of the eigenvalues. Van Leer [8] proposed a new form of splitting which makes each split flux continuously differentiable and also degenerate for $|u'| < c$. The latter condition produces one zero eigenvalue for the split flux Jacobians, leading to steady transonic shock structures with only two interior zones. Equation (49) is still assumed valid for $|u'| \geqslant c$. For $|u'| < c$, the requirement of continuous differentiability leads to the presence of a factor $(u' \pm c)^2$ in the formula for $F_n^{\pm}$, respectively. The simplest splitting of the mass flux satisfying certain symmetry conditions gives

$$M^{\pm} = \pm \frac{\rho}{4c} (u' \pm c)^2. \tag{50}$$

The splitting of the momentum flux takes the form

$$\mathbf{P}^{\pm} = M^{\pm} \left[\mathbf{u} - \frac{1}{\gamma} (u' \mp 2c) \mathbf{n} \right]. \tag{51}$$

Note that Eqs. (50) and (51) are valid for a general gas law, with $\gamma \equiv \rho c^2/p$. In order to satisfy the degeneracy condition, the split energy flux must satisfy

$$E^{\pm} = f(M^{\pm}, \mathbf{P}^{\pm}, \mathbf{n}, \mathbf{v}). \tag{52}$$

One can show that this is only possible for a perfect gas. The resulting expression is

$$E\pm = M^{\pm} \left[\frac{\{(\gamma - 1) u' \pm 2c\}^2}{2(\gamma^2 - 1)} - \frac{v_n}{\gamma} (u' \mp 2c) + \frac{1}{2} (\mathbf{u} \cdot \mathbf{u} - u'^2) \right]. \tag{53}$$

Discretization of Conservation Laws

Spatial Discretization

A primary grid is defined by choosing a set of discrete grid points and connections among them. Normally points are chosen to lie on the flow region boundaries. The grid also divides the region into a set of contiguous primary cells, where the grid points are now cell vertices and the connections form the edges of the faces common to neighboring cells. If the shapes of the connections are not precisely given, then the edges are not defined uniquely. Normally the connections are specified as straight lines. Even when the shapes of the connections are given, the shapes of the faces are not uniquely defined in three dimensions. For ordered grids the cells are quadrilaterals in two dimensions and hexahedrons in three dimensions. Grid points may be specified numerically or analytically. In time-dependent algorithms the grid points can advance in time.

A secondary grid can be obtained by determining the centers or centroids of the primary cells (in a non-unique way) and connecting them across cell faces. The secondary grid points also act as vertices of secondary cells. We thus have two interlocking grids, with the cell vertices of one being the cell centers of the other. One should note that if the primary grid is not sufficiently smooth, a secondary grid with straight line connections may not be possible. One can always define a secondary grid with piecewise straight connections by determining the centers of the faces of each primary cell and connecting them to the cell center with straight lines. The role of grids in the finite-difference and finite-volume discretization of the equations is examined below. The discussion focuses primarily on stationary grids at interior points. The case of moving grids as well as considerations at flow region boundaries are covered in subsequent sections.

Finite-Difference Discretization

Standard finite-difference methods are based on the discretization of Eq. (20), with the geometric quantities included in the definitions of the transformed variables. The position vector $\mathbf{r}$ and the primary variable Q are defined at the primary grid points corresponding to equispaced points in the computational ξ, η, ζ space. The geometric quantities defined by Eqs. (14)–(18) are evaluated at each grid point from the $\mathbf{r}$ data by central-difference approximations. At interior points, a conservative difference algorithm is applied in terms of the transformed variables defined in Eq. (20). If i, j, k are the integer indices corresponding to the ξ, η, ζ coordinates, the spatial difference approximation can always be expressed in the form

$$(\hat{F}^{\xi})_{\xi} = (\hat{F}^{\xi}_{i+1/2,j,k} - \hat{F}^{\xi}_{i-1/2,j,k})/\Delta\xi, \tag{54}$$

where $\hat{F}^{\xi}_{i+1/2,j,k}$ is any numerical approximation to the flux across the $i+\frac{1}{2}$, j, k face of the secondary grid. Similar relations hold for the η and ζ derivatives. The numerical flux can be obtained by central differences or by any of the varieties of upwind methods. It can also contain additional artificial terms to stabilize the calculation. The time integration of Eq. (20) can be explicit or implicit, may involve dimensional splitting, and can involve time linerization to avoid iteration during a time step. In the latter instance, the matrix A of Eq. (29) is evaluated at the primary grid points.

The form of Eq. (54) guarantees that when Eq. (20) is summed over all the grid points, interior flux terms will cancel. This telescoping property defines conservative differencing. For unsteady flow, the summation implies that $\hat{U}_{i,j,k}$ is an approximation to the conserved variable contained in a secondary cell surrounding the primary grid point i, j, k. These considerations must be modified for those grid points that lie on the flow region boundaries. First of all, the geometric quantities must be evaluated using one-sided differences. The flow variables U are calculated by applying appropriate boundary conditions. These involve auxiliary equations or

characteristic relations which determine which quantities are specified and which are related to interior quantities in some manner.

It is seen that the standard finite-difference approach combines geometric and flow variables and subjects the resultant transformed variables to an algebraic treatment. The flow variables are unknown and can only be determined within some truncation errors. On the other hand, for a given coordinate transformation the geometric variables obey their own identities which could be satisfied exactly. The combined approach can give rise to numerical errors even when the flow is known exactly. These will be discussed in more detail in subsequent sections. Some of the sources of inaccuracies are:

1. The geometric identities (21) and (22) may not be precisely satisfied. Since the surface area vectors are linear functions of the position vectors in two dimensions, the discrete form of Eq. (21) will have no truncation error in this case when central differences are used throughout. However, in three dimensions the area vectors are quadratic functions of the position vectors. Since the product of two averages is not equal to the average of two products, truncation errors will be present in this case. As a result, the time integration of a uniform flow will result in numerical oscillations. The discretization of Eq. (15) will result in secondary cell volumes that will not sum to the total volume of the flow region. This can be a source of error in unsteady flow calculations. If the grid is undergoing deformation with time ($\mathbf{v}_c \neq 0$), the discrete form of Eq. (22) will in general not be satisfied, irrespective of how V and $\mathbf{r}_\tau$ are evaluated. This will give rise to errors in a uniform flow even in two dimensions. If the numerical flux is obtained by an upwind method, the geometric variables are not treated in a fully centered way. This also can produce numerical errors, even in two dimensions.

2. The calculation of derivatives from Eqs. (17)–(19) can give rise to inaccuracies. In potential flow, where Q is the velocity potential, the gradient of Q is the fluid velocity and therefore must be determined accurately. If the difference approximation for Q_ξ is not consistent with that for $\nabla\xi$ based on geometric quantities at the primary grid points, the calculation of ∇Q from Eq. (17) will result in errors in a uniform flow. Similarly, for unsteady potential flow with moving grids, the time differencing of Q_τ and $\mathbf{r}_\tau$ must be consistent in order to avoid further errors from the use of Eq. (19). For the Navier–Stokes equations, an inaccuracy of a different kind is possible. If a central difference approximation for ∇Q from Eq. (17) is used to calculate the transport terms in the numerical fluxes of Eq. (54), the derivative $(\hat{F}^\xi)_\xi$ at the grid point i, j, k will depend on the position vectors $\mathbf{r}$ at the points $i+2, j, k$ and $i-2, j, k$. This lack of compactness puts more stringent requirements on the smoothness of the grid in order to achieve a desired accuracy.

3. The treatment of boundary points can also be a source of inaccuracies. The evaluation of geometric quantities by one-sided differences is inconsistent with the central difference approximation used at the neighboring interior point, resulting in a possible loss of accuracy. If a grid singularity occurs on the boundary, the ordinary difference procedure can give a large error. The boundary procedure used

to evaluate the flow variables at a boundary grid point may not explicitly satisfy Eq. (20), which is used at the neighboring interior point. This inconsistency can also be a source of error.

In a practical finite-difference code these numerical errors are handled in two ways. Specific corrections can be applied to cancel errors in a uniform flow. The standard finite-difference discretization can also be modified to treat the geometric terms more precisely. Both of these procedures are discussed in more detail in the comparisons with the finite-volume discretization presented below. Further discussions of geometrically induced errors are found in subsequent sections on moving grids and treatment of boundaries.

Finite-Volume Geometry

As a building block for subsequent calculations, we consider a triangular face whose vertices are $\mathbf{r}_1$, $\mathbf{r}_2$, and $\mathbf{r}_3$. A properly oriented surface area vector for that face is given by

$$\mathbf{S}_{123} = S_{123}\mathbf{n}_{123} = \int_{123} \mathbf{n}\, dS = \tfrac{1}{2}(\mathbf{r}_2 - \mathbf{r}_1) \times (\mathbf{r}_3 - \mathbf{r}_1). \tag{55}$$

The formula implies that the edges are straight lines connecting the vertices, and that the face is the plane determined by the three vertices. Actually, it follows from Eq. (6) that the surface area vector is only a function of the shapes of the edges. Thus Eq. (55) is valid for *any* face with straight line edges. Further reflection reveals that there are an infinite number of edge shapes connecting two vertices that will give the same surface area vector as a straight line. These shapes can be called equivalent straight line shapes. Thus Eq. (55) is valid for any triangular face with equivalent straight line connections.

Let a multiply subscripted position vector denote the vectorial average of the individual vectors. Thus

$$\mathbf{r}_{123} \equiv \tfrac{1}{3}(\mathbf{r}_1 + \mathbf{r}_2 + \mathbf{r}_3) \tag{56}$$

is the center of the face. One can easily show that for a plane face with straight line edges

$$\int_{123} \mathbf{r}\, dS = S_{123}\mathbf{r}_{123}, \tag{57}$$

i.e., the centroid is located at the center. Note that this is not valid if the edges deviate from straight lines. From Eq. (8) it follows that the moment of the area

$$\mathbf{M}_{123} \equiv \int_{123} \mathbf{r} \times \mathbf{n}\, dS = S_{123}\mathbf{r}_{123} \times \mathbf{n}_{123} \tag{58}$$

for any face with straight line edges. For a tetrahedral cell with vertices $\mathbf{r}_1$, $\mathbf{r}_2$, $\mathbf{r}_3$, and $\mathbf{r}_4$, defined by plane faces and straight edges, the volume is given by

$$V_{1234} = \tfrac{1}{6}(\mathbf{r}_2 - \mathbf{r}_1) \times (\mathbf{r}_3 - \mathbf{r}_1) \cdot (\mathbf{r}_4 - \mathbf{r}_1) = \tfrac{1}{3}\mathbf{S}_{123} \cdot (\mathbf{r}_4 - \mathbf{r}_1). \tag{59}$$

The above formulas can be used to make geometric calculations for an arbitrary cell with straight line edges. Each polygonal face can be subdivided into plane triangular facets and the total volume treated as a sum of tetrahedra. The resulting surface area vectors and their moments for each face are unique, but the total volume will depend on the method of subdivision. Calculations for a regular hexahedral cell are presented below.

A hexahedron defined by eight vertices is shown in Fig. 1, with edges 14, 12, and 15 directed in the positive ξ, η, and ζ directions, respectively. The surface area vectors in the positive ξ direction are $\mathbf{S}_{1562}$ and $\mathbf{S}_{4873}$, as indicated. The expression for the former can be written with the aid of Eq. (55) as

$$\mathbf{S}_{1562} = \tfrac{1}{2}(\mathbf{r}_6 - \mathbf{r}_1) \times (\mathbf{r}_5 - \mathbf{r}_2) \tag{60a}$$

$$= (\mathbf{r}_{56} - \mathbf{r}_{12}) \times (\mathbf{r}_{15} - \mathbf{r}_{26}). \tag{60b}$$

The more efficient form (60a) is expressed as the vector product of the two diagonals, showing that each diagonal is perpendicular to the surface normal. The form (60b) is in terms of the two vectors joining opposite edge midpoints. Since these vectors intersect in the face center $\mathbf{r}_{1562}$, it follows that the four edge midpoints and the face center all lie in a plane midway between the planes containing the two diagonals. The moment of the area is obtained by dividing the face along one diagonal and can be written as

$$\mathbf{M}_{1562} = \int_{1562} \mathbf{r} \times \mathbf{n}\, dS = \mathbf{r}_{165} \times \mathbf{S}_{165} + \mathbf{r}_{126} \times \mathbf{S}_{126}. \tag{61}$$

In order to ensure that the volumes of the hexahedrons sum to the total volume,

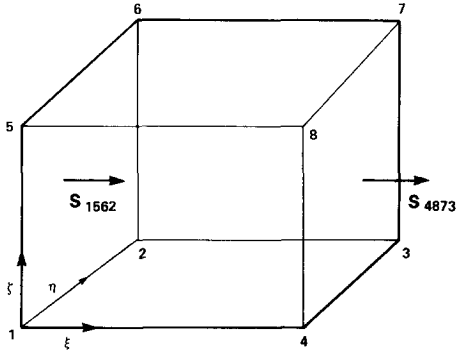

FIG. 1. Geometry of hexahedral cell.

the shape of each face must be precisely defined and consistently used by the two neighboring cells. A simple way to calculate the cell volume is to choose an arbitrary point inside the cell. The volume is just the sum of the volumes of six pyramids, each with one face as the base and the arbitrary point as the common apex. For each non-planar face there exists the location of an equivalent plane face which gives the same volume for the pyramid. In fact, there are an infinite number of face shapes corresponding to a given equivalent plane face. The volume of the pyramid is then one-third of the dot product of the surface area vector of the face and a vector from the apex to any point lying in the equivalent plane.

The earliest expression for the volume of a hexahedron, based on an equivalent plane face containing a diagonal, was given by Rizzi [9]. Unfortunately the equivalent planes for a pair of opposite faces contain oppositely oriented diagonals, so that the volumes do not sum properly. Kordulla and Vinokur [10] showed that of the eight consistent divisions of the faces by diagonals, four result in a very simple expression for the volume. If one vertex of a cell main diagonal is chosen as the common apex and the other vertex as the intersection of three equivalent plane faces, the six pyramids reduce to three pyramids sharing the main diagonal as a common edge. Using the second form of Eq. (59), one obtains the expression

$$V_{12345678} = \tfrac{1}{3}(\mathbf{S}_{1485} + \mathbf{S}_{1234} + \mathbf{S}_{1562}) \cdot (\mathbf{r}_7 - \mathbf{r}_1). \tag{62}$$

Three similar expressions can be derived based on the other three choices for main diagonal, each yielding a different value for the volume.

An alternate expression for the volume is based on the equivalent plane face passing through the edge midpoints and face center. Formulas using face centers to calculate the volumes of the six pyramids were proposed by Jameson [11] and Holmes and Tong [12]. It was shown by Davies and Salmond [13] that the same equivalent plane corresponds to a face defined as a doubly ruled surface. Edge midpoints were used to obtain more efficient expressions for the cell volume, but full efficiency was not obtained since a cell vertex was chosen as the common apex. If the edge midpoint $\mathbf{r}_{12}$ is chosen as the common apex and $\mathbf{r}_{67}$ and $\mathbf{r}_{48}$ are each at the intersection of two equivalent plane faces, one obtains the more efficient expression.

$$V_{12345678} = \tfrac{1}{3}[(\mathbf{S}_{5678} + \mathbf{S}_{2376}) \cdot (\mathbf{r}_{67} - \mathbf{r}_{12}) + (\mathbf{S}_{1458} + \mathbf{S}_{4873}) \cdot (\mathbf{r}_{48} - \mathbf{r}_{12})]. \tag{63}$$

It can be shown that the volume given by Eq. (63) is the average of the volumes determined by the eight consistent divisions of the cell faces by diagonals.

For completeness we give the geometric expressions for 2-dimensional and axisymmetric flow. The volume element is now defined by the co-planar vertices $\mathbf{r}_1$, $\mathbf{r}_2$, $\mathbf{r}_3$, and $\mathbf{r}_4$, where $\mathbf{k}$ is the unit normal to the plane. For 2-dimensional flow the surface area vectors take the form

$$\mathbf{S}_{12} = (\mathbf{r}_2 - \mathbf{r}_1) \times \mathbf{k}, \qquad \mathbf{S}_{23} = (\mathbf{r}_2 - \mathbf{r}_3) \times \mathbf{k}, \tag{64}$$

while the area moments become

$$\mathbf{M}_{12} = \int_{12} \mathbf{r} \times \mathbf{n}\, dS = \tfrac{1}{2}(\mathbf{r}_1 \cdot \mathbf{r}_1 - \mathbf{r}_2 \cdot \mathbf{r}_2)\mathbf{k},$$
$$\mathbf{M}_{23} = \int_{23} \mathbf{r} \times \mathbf{n}\, dS = \tfrac{1}{2}(\mathbf{r}_3 \cdot \mathbf{r}_3 - \mathbf{r}_2 \cdot \mathbf{r}_2)\mathbf{k}. \tag{65}$$

The volume is given by

$$V_{1234} = \tfrac{1}{2}(\mathbf{r}_3 - \mathbf{r}_1) \times (\mathbf{r}_2 - \mathbf{r}_4) \cdot \mathbf{k}. \tag{66}$$

For axisymmetric flow, let y be the distance from the axis of symmetry. The surface area vectors (per unit circumferential angle) are

$$\mathbf{S}_{12} = y_{12}(\mathbf{r}_2 - \mathbf{r}_1) \times \mathbf{k}, \qquad \mathbf{S}_{23} = y_{23}(\mathbf{r}_2 - \mathbf{r}_3) \times \mathbf{k}, \tag{67}$$

while the lateral surface area vector becomes

$$\mathbf{S}_{1234} = \tfrac{1}{2}(\mathbf{r}_3 - \mathbf{r}_1) \times (\mathbf{r}_2 - \mathbf{r}_4). \tag{68}$$

The volume (per unit circumferential angle) can be obtained from

$$V_{1234} = \tfrac{1}{2}[y_{132}(\mathbf{r}_3 - \mathbf{r}_1) \times (\mathbf{r}_2 - \mathbf{r}_1) + y_{134}(\mathbf{r}_4 - \mathbf{r}_1) \times (\mathbf{r}_3 - \mathbf{r}_1)] \cdot \mathbf{k}. \tag{69}$$

Finite-Volume Discretization

Finite-volume methods are based on the discretization of Eq. (1), with the surface integral replaced by the sum of integrals over the faces of the cell. The method is normally applied to cells defined by the primary grid, so that certain cell faces will coincide with the flow region boundary. One can also apply the method to secondary cells, in which case the boundary cells are not full cells. The discussion is limited to ordered grids, but much of it can be extended to general grids. A full set of integer subscripts refers to a cell, or the center or centroid of a cell. Fractional subscripts then indicate cell faces, edges, or vertices. Thus the cell is defined by specifying the vertices (e.g., $\mathbf{r}_{i+1/2,j+1/2,k+1/2}$), and these are used to calculate surface area vectors (e.g., $\mathbf{S}^{\xi}_{i+1/2,j,k}$), area moments, and the cell volume $V_{i,j,k}$ using the formulas derived above. This ensures that all the geometric identities and constraints are precisely satisfied. If $\mathbf{F}$ is spatially uniform (which is valid for a uniform free stream), the numerical calculation of the surface integral for each face should sum to zero (within roundoff errors). This is a necessary condition for the preservation of a free stream. Temporal discretization is given by the superscripts n and $n+1$, which refer to times t_1 and t_2, respectively.

The primary variable Q is normally associated with the cell or cell center. In some algorithms, such as that of Tong [14], it is defined at cell vertices. While these schemes offer better accuracy for grids that are not smooth, their practical

implementation is limited to steady-state flows governed by the Euler equations. In other algorithms for these flows [15, 16], Q is the average value on a cell face. Only the first case is treated here. We first consider a flow governed by the full set of conservation laws, for which U is a function of Q. All spatial integrals are replaced by the product of the spatial quantity and the average value of the integrand. Thus the geometry of the discretization is treated separately from the treatment of the physical variables. There is a certain ambiguity in the interpretation of $U_{i,j,k}$ in the relation

$$\int_{V_{i,j,k}} U\, dV = U_{i,j,k} V_{i,j,k}. \tag{70}$$

Strict equality implies that $U_{i,j,k}$ is the average value of U in the cell. But in order to calculate a surface flux it is convenient to think of $U_{i,j,k}$ as the value of U at some average point in the cell, with the $=$ sign replaced by the $\approx$ sign. This interpretation of $U_{i,j,k}$ is also implied when one uses the equation of state to express the pressure in terms of the conservative variables. A characteristic of the finite-volume method is that the precise location of this average point is not required during the calculation. Only in the output of the solution is a location of this point desired. Some investigators have suggested the cell centroid for this point. This is strictly valid only if all the components of U vary linearly throughout the cell. Since the distribution of U is not known, the centroid has no particular advantage over the cell center, defined as the vectorial average of the cell vertices. The latter point is easier to calculate and is therefore preferable. Of course, when the finite-volume method is applied to a secondary cell, the primary grid point is available as the average point for the cell.

The major problem in a finite-volume method is the calculation of the time integral of the average flux over each face. The time integral can be approximated as

$$\int_{t_1}^{t_2} \hat{F}^{\xi}_{i+1/2,j,k}\, dt \approx [(1-\theta)(\hat{F}^{\xi}_{i+1/2,j,k})^n + \theta(\hat{F}^{\xi}_{i+1/2,j,k})^{n+1}]\, \Delta t, \tag{71}$$

where

$$\hat{F}^{\xi}_{i+1/2,j,k} \equiv \int_{\mathbf{S}^{\xi}_{i+1/2,j,k}} \mathbf{n}\cdot\mathbf{F}\, dS \approx \mathbf{S}^{\xi}_{i+1/2,j,k}\cdot\mathbf{F}_{i+1/2,j,k}, \tag{72}$$

and $\Delta t = t_2 - t_1$. For implicit time integration ($\theta \neq 0$), $\mathbf{F}^{n+1}_{i+1/2,j,k}$ is not known and is therefore linearized about time level n. On the other hand, for a cell face that varies with time, $(\mathbf{S}^{\xi}_{i+1/2,j,k})^{n+1}$ is known and need not be linearized. This is one distinction between the finite-difference and finite-volume approach which is discussed further in the next section. The calculation of the average flux is now presented for each of the class of equations, with comparisons between the finite-difference and finite-volume methods made in each case.

Euler Equations

For the Euler equations, one only needs the inviscid part of the average flux. The numerical procedures for this case can be divided into three classes. In the first class $\mathbf{F}_{i+1/2,j,k}$ depends only on $U_{i,j,k}$ and $U_{i+1,j,k}$, but requires an additional artificial smoothing flux to stabilize the calculation. This class includes multi-step algorithms in which $\mathbf{F}_{i+1/2,j,k}$ is alternately $\mathbf{F}_{i,j,k}$ and $\mathbf{F}_{i+1,j,k}$, where

$$\mathbf{F}_{i,j,k} \equiv \mathbf{F}(U_{i,j,k}), \tag{73}$$

and single step centered approximations of the form

$$\mathbf{F}_{i+1/2,j,k} = \tfrac{1}{2}(\mathbf{F}_{i,j,k} + \mathbf{F}_{i+1,j,k}). \tag{74}$$

Another form for the centered approximation is

$$\mathbf{F}_{i+1/2,j,k} = \mathbf{F}(U_{i+1/2,j,k}), \tag{75}$$

where

$$U_{i+1/2,j,k} = \tfrac{1}{2}(U_{i,j,k} + U_{i+1,j,k}). \tag{76}$$

Form (75) is probably more consistent with the spirit of a finite-volume formulation. As discussed in [12], it gives better results near solid wall boundaries. It has the disadvantage of requiring three times as many flux evaluations in three dimensions as does (74). As an alternative, a form based on Eq. (2) has been suggested [12, 17]. (We are treating the case $\mathbf{v} = 0$ for now.) It can be written as

$$\mathbf{F}_{i+1/2,j,k} = \mathbf{u}_{i+1/2,j,k} U_{i+1/2,j,k} + \tfrac{1}{2}(\mathbf{G}_{i,j,k} + \mathbf{G}_{i+1,j,k}), \tag{77}$$

where

$$\mathbf{u}_{i+1/2,j,k} = \tfrac{1}{2}(\mathbf{u}_{i,j,k} + \mathbf{u}_{i+1,j,k}). \tag{78}$$

This produces the favorable behavior of form (75) with less computing effort.

The approximations to the flux integrals for the two faces in the ξ direction based on Eq. (74) take the form

$$\tfrac{1}{2}[\mathbf{S}^{\xi}_{i+1/2,j,k} \cdot (\mathbf{F}_{i,j,k} + \mathbf{F}_{i+1,j,k}) - \mathbf{S}^{\xi}_{i-1/2,j,k} \cdot (\mathbf{F}_{i-1,j,k} + \mathbf{F}_{i,j,k})]. \tag{79}$$

The analogous finite-difference expression is

$$\tfrac{1}{2}[\mathbf{S}^{\xi}_{i+1,j,k} \cdot \mathbf{F}_{i+1,j,k} - \mathbf{S}^{\xi}_{i-1,j,k} \cdot \mathbf{F}_{i-1,j,k}]. \tag{80}$$

Note that Eq. (80) is simpler than Eq. (79), since it contains fewer terms. Yet the conservation that it implies is carried out over a wider region. Specifically, the numerical telescoping property is valid over a distance of two cell widths in each direction. Thus conservation in a finite-difference discretization is effectively carried

out over eight sets of overlapping cells with double the size in each direction of the original cells. This could lead to larger errors for grids that are not smooth, and near flow region boundaries.

Another source of error in the standard finite-difference discretization for three dimensions is the central difference approximation to the surface area vector such as $\mathbf{S}^{\xi}_{i+1,j,k}$. This will result in oscillations for a uniform flow since Eq. (6) is not satisfied for the doubly sized cell. This was discussed in [3, 18]. An appropriate difference formula, equivalent to the application of Eq. (60b) to the larger cell, was presented in [18]. A more efficient formula was given in [3]. Actually, the most efficient form is derived from Eq. (60a) as

$$\mathbf{S}^{\xi}_{i+1,j,k} = \tfrac{1}{8}(\mathbf{r}_{i+1,j+1,k+1} - \mathbf{r}_{i+1,j-1,k-1}) \times (\mathbf{r}_{i+1,j-1,k+1} - \mathbf{r}_{i+1,j+1,k-1}). \tag{81}$$

This takes no more operations than the central difference formula and eliminates errors for a uniform flow. For problems in which the free stream is a uniform flow, an alternate procedure suggested in [18] is to subtract the free-stream fluxes from the conservation equations. This will guarantee exact cancellation of free-stream errors resulting from the central difference approximation to $\mathbf{S}^{\xi}_{i+1,j,k}$.

To circumvent the need for artificial smoothing fluxes with the first class of approximations, upwind-biased approximations that model the waves crossing the face are required. For the face with surface area vector $\mathbf{S}^{\xi}_{i+1/2,j,k} = S^{\xi}_{i+1/2,j,k}\mathbf{n}^{\xi}_{i+1/2,j,k}$, we introduce the notation $F^{\xi} = \mathbf{n}^{\xi}_{i+1/2,j,k} \cdot \mathbf{F}$ for the normal flux component. In order to achieve higher than first-order spatial accuracy, an upwind-biased numerical flux $F^{\xi}_{i+1/2,j,k}$ depends on states other than $U_{i,j,k}$ and $U_{i+1,j,k}$. There are two ways this is generally accomplished. Probably closer to the finite-volume philosophy is the class of approximations associated with the name MUSCL, in which the final calculation is only in terms of quantities defined at the face. If $U^{-}_{i+1/2,j,k}$ and $U^{+}_{i+1/2,j,k}$ are conservative variables just on the negative and positive sides of the face, then the numerical flux is given by an expression of the form

$$F^{\xi}_{i+1/2,j,k} = f(U^{-}_{i+1/2,j,k}, U^{+}_{i+1/2,j,k}, \mathbf{n}^{\xi}_{i+1/2,j,k}). \tag{82}$$

For first-order accuracy, $U^{-}_{i+1/2,j,k} = U_{i,j,k}$. For higher order spatial accuracy, if dimensional splitting is employed, $U^{-}_{i+1/2,,k}$ is obtained from upwind-biased interpolation of $U_{i-1,j,k}$, $U_{i,j,k}$, and possibly $U_{i+1,j,k}$, where the coefficients may be modified using appropriate limiters to prevent numerical oscillations. Analogous formulas give $U^{+}_{i+1/2,j,k}$. Examples of a higher order calculation without dimensional splitting for two dimensions may be found in [19, 20].

One form of (82) that represents the physics of the wave processes is the 1-dimensional Riemann solver for the two constant states $U^{-}_{i+1/2,j,k}$ and $U^{+}_{i+1/2,j,k}$. This gives a unique value for $U_{i+1/2,j,k}$ at the face and the resultant numerical flux

$$F^{\xi}_{i+1/2,j,k} = F^{\xi}(U_{i+1/2,j,k}). \tag{83}$$

Since an exact Riemann solver is iterative, and computationally expensive, approximate Riemann solvers have been devised, such as those of Godunov [21], Osher and Solomon [22], Collela [23], Montagné [24], Pandolfi [25], and Dukowics [26].

An algebraic approach to obtain (82) is that of flux-vector splitting. For the Steger–Warming and Van Leer splittings, which are given in the previous section, the solution is

$$F^{\xi}_{i+1/2,j,k} = F^{\xi+}(U^{-}_{i+1/2,j,k}) + F^{\xi-}(U^{+}_{i+1/2,j,k}). \tag{84}$$

Calculations using both these splittings for an implicit factored algorithm are presented in [27]. Similar calculations using the splitting of Eq. (45) are found in [6] for an implicit algorithm, and in [28, 29] for a two-step explicit algorithm. Implicit finite-difference calculations using the Steger–Warming splitting are carried out in [30]. Here free-stream fluxes are again subtracted in order to eliminate errors in a uniform flow.

A third appraoch is based on a local linearization due to Huang [31] and Roe [5]. In terms of the operator $A_{i+1/2,j,k} \equiv A(U_{i+1/2,j,k})$ for some average $U_{i+1/2,j,k}$, the solution can be written in the form

$$\begin{aligned} F^{\xi}_{i+1/2,j,k} = \tfrac{1}{2}[&F^{\xi}(U^{-}_{i+1/2,j,k}) + F^{\xi}(U^{-}_{i+1/2,j,k}) \\ &- |A_{i+1/2,j,k}|\,(U^{+}_{i+1/2,j,k} - U^{-}_{i+1/2,j,k})]. \end{aligned} \tag{85}$$

The last term can be interpreted as a dissipative correction to a centered approximation, with $A_{i+1/2,j,k}$ acting as a numerical viscosity operator. Since (85) violates an entropy inequality, the actual form that is used is modified in some manner in order to prohibit non-physical solutions. Theoretically, the optimum choice for $U_{i+1/2,j,k}$ is the Roe average of $U^{+}_{i+1/2,j,k}$ and $U^{-}_{i+1/2,j,k}$, given in the previous section, but eqaully satisfactory results are usually obtained if the simpler arithmetic average is used. The results of the other two approaches can also be written in a form analogous to (85). For example, Eq. (84) for Steger–Warming flux splitting can be written as (85), with the dissipation term replaced by

$$|A(U^{+}_{i+1/2,j,k})|\,U^{+}_{i+1/2,j,k} - |A(U^{-}_{i+1/2,j,k})|\,U^{-}_{i+1/2,j,k}. \tag{86}$$

The other class of higher order upwind-biased approximations to the numerical flux at a cell face involves the consideration of the wave processes at neighboring faces. This can be done using any of the three approaches described above to represent the wave processes. There is some question as to how the geometry of the neighboring face should enter the calculation. From a strict finite-volume viewpoint, all calculations relating to the determination of $F^{\xi}_{i+1/2,j,k}$ should only involve $\mathbf{n}^{\xi}_{i+1/2,j,k}$, even at neighboring faces. This is computationally expensive and does not take into account the grid curvature. It is therefore more appropriate to use the local face normal in calculations involving parameters defined at neighboring faces. The local geometric scale of the neighboring face can also be involved. To illustrate

this we consider the application of the local linearization approach. In the scheme of [32], one requires flux differences across neighboring faces, modified by appropriate limiters. The relevant parameters defined for face $i+\frac{1}{2}, j, k$ are the components of

$$S_{i+1/2,j,k} R^{-1}_{i+1/2,j,k} [F^{\xi}(U_{i+1,j,k}) - F^{\xi}(U_{i,j,k})]. \tag{87}$$

In the modified flux approach of Harten [33, 34], as implemented for curvilinear coordinates in [35], the relevant parameters are the components of

$$V_{i+1/2,j,k} R^{-1}_{i+1/2,j,k} (U_{i+1,j,k} - U_{i,j,k}), \tag{88}$$

where $V_{i+1/2,j,k}$ is some average of the volumes of the two adjoining cells. The two different geometric scales arise naturally from the extension of a Cartesian analysis to curvilinear coordinates using Eq. (20). In the finite-volume upwind scheme of Coakley [36], the parameters are those of Eq. (88) without the geometric scale (i.e., $V_{i+1/2,j,k} = 1.$) Further numerical experiments should be conducted to determine which geometric scale (or none at all) gives the best results.

Navier–Stokes Equations

The calculation of transport terms in the average flux for the Navier–Stokes equations necessitates the evaluation of ∇Q. This can be done using the nonconservative expression (17), or basing it on the conservative definition

$$\int_V \nabla Q \, dV = \oint_S \mathbf{n} Q \, dS. \tag{89}$$

The second form leads to a more complex expression, but is more consistent with the finite-volume philosophy. It also has some computational advantages, which will be indicated presently. Applying Eq. (89) to an auxiliary cell centered at $i+\frac{1}{2}, j, k$, one obtains

$$(\nabla Q)_{i+1/2,j,k} = (\mathbf{S}^{\xi}_{i+1,j,k} Q_{i+1,j,k} - \mathbf{S}^{\xi}_{i,j,k} Q_{i,j,k} + \mathbf{S}^{\eta}_{i+1/2,j+1/2,k} Q_{i+1/2,j+1/2,k} - \mathbf{S}^{\eta}_{i+1/2,j-1/2,k} Q_{i+1/2,j-1/2,k}$$

The geometric terms in Eq. (90) can be obtained in two ways. The vertices of the auxiliary cell can be defined as vectorial averages of the vertices of the original cells, and the exact expressions for areas and volumes can then be applied to them. Since true conservation for the auxiliary cells is not required, the averages of the areas and volumes of the original cells can be used directly to define the corresponding quantities for the auxiliary cell. The second method is more efficient, particularly for three dimensions.

The values of Q in the first two terms, corresponding to the longitudinal component of the gradient, are already given. The remaining values, which contribute to the transverse components, must be determined by suitable averages. For example, one can define $Q_{i+1/2,j+1/2,k}$ as

$$Q_{i+1/2,j+1/2,k} = \tfrac{1}{4}(Q_{i,j+1,k} + Q_{i+1,j+1,k} + Q_{i,j,k} + Q_{i+1,j,k}). \tag{91}$$

The sum of the contributions of the last four terms in Eq. (90) using Eq. (91) for Cartesian coordinates does not involve $Q_{i,j,k}$ or $Q_{i+1,j,k}$. If relaxation methods are used to advance the solution in time implicitly, these terms will affect the diagonal dominance of the iteration matrix only weakly due to the nonuniformity of the grid. On the other hand, if $Q_{i+1/2,j+1/2,k}$ is defined as

$$Q_{i+1/2,j+1/2,k} = \tfrac{1}{2}(Q_{i,j+1,k} + Q_{i+1,j,k}) \tag{92a}$$

or

$$Q_{i+1/2,j+1/2,k} = \tfrac{1}{2}(Q_{i+1,j+1,k} + Q_{i,j,k}), \tag{92b}$$

the last four terms in Eq. (90) can be combined to improve the diagonal dominance. This was pointed out in [37], where criteria are given on the use of Eq. (92a) or (92b).

The nonconservative form of $(\nabla Q)_{i+1/2,j,k}$ based on Eq. (17) is usually applied in the thin-layer approximation, with the transverse components neglected. Using Eq. (18), it can be written as

$$(\nabla Q)_{i+1/2,j,k} \approx \mathbf{S}^{\xi}_{i+1/2,j,k}(Q_{i+1,j,k} - Q_{i,j,k})/V_{i+1/2,j,k}, \tag{93}$$

with a simple average defining $V_{i+1/2,j,k}$. If the transverse terms are required, they can be written in several different ways, using expressions such as

$$(\nabla \eta)_{i,j,k} = \mathbf{S}^{\eta}_{i,j,k}/V_{i,j,k}, \tag{94}$$

with a simple average now defining $\mathbf{S}^{\eta}_{i,j,k}$. Note that the transverse terms do not affect the diagonal dominance in the nonconservative form. All the above relations for the gradient can be used for the transpose by reversing the order of the terms in all products. The divergence is obtained by employing a dot product for all the products.

The nonconservative form of a transport term can be related to the analogous finite-difference expression. Consider a flux of the form $\alpha \nabla Q$, where α is a scalar function of Q. For the longitudinal component of the flux integral over face $i+\frac{1}{2}, j, k$, the finite-volume expression is

$$(\alpha/V)_{i+1/2,j,k}\mathbf{S}^{\xi}_{i+1/2,j,k} \cdot \mathbf{S}^{\xi}_{i+1/2,j,k}(Q_{i+1,j,k} - Q_{i,j,k}), \tag{95}$$

where $(\alpha/V)_{i+1/2,j,k}$ is defined by a simple average. The analogous finite-difference expression is

$$\tfrac{1}{2}(\alpha_{i,j,k}\mathbf{S}^{\xi}_{i,j,k}\cdot\mathbf{S}^{\xi}_{i,j,k}/V_{i,j,k}+\alpha_{i+1,j,k}\mathbf{S}^{\xi}_{i+1,j,k}\cdot\mathbf{S}^{\xi}_{i+1,j,k}/V_{i+1,j,k})(Q_{i+1,j,k}-Q_{i,j,k}). \tag{96}$$

It is interesting to compare these two equations (and the corresponding ones for face $i-1/2$, j, k) with Eqs. (79) and (80) that relate the inviscid flux integrals. We first note that the finite-volume expression (95) is now a little simpler. A more significant factor is the presence of the volumes in the flux integrals required to calculate the gradients. If a central difference approximation is used to determine the volumes using Eq. (15), the contributions of the finite-difference flux integrals for cell i, j, k involve the position vectors $\mathbf{r}_{i+2,j,k}$ and $\mathbf{r}_{i-2,j,k}$. Thus the dependence on the grid geometry due to the transport terms is less compact. This could lead to additional errors for grids that are not smooth and near flow region boundaries. One also notes that the numerical telescoping of the finite-difference transport flux terms is with adjacent cells. It is thus inconsistent with the telescoping of the inviscid terms. Since the transport terms give no contribution for a uniform flow, they play no role in satisfying Eq. (6). One can thus use Eq. (81) to calculate surface area vectors appearing in Eq. (96). Similar conclusions can be obtained for other forms of the flux representing transport terms. The transverse component of the flux integral has the same behavior as the inviscid flux integral and has the same telescoping property. It does exhibit the lack of compactness of the longitudinal component due to the presence of the volumes.

Potential Flow

Another important case where gradients must be calculated is potential flow. For an irrotational flow the velocity is given by

$$\mathbf{u}=\nabla\phi, \tag{97}$$

where ϕ is the velocity potential. If one further assumes the flow is isentropic, the momentum equation has the general Bernoulli integral

$$h=C(\tau)-\phi_{\tau}-\tfrac{1}{2}\nabla\phi\cdot\nabla\phi+\nabla\phi\cdot\mathbf{r}_{\tau}. \tag{98}$$

Here $h=\varepsilon+p/\rho$ is the specific enthalpy and $C(\tau)$ is an arbitrary function of τ. In most problems C is a constant. An arbitrary coordinate transformation has been included. The integral is valid for an arbitrary equation of state. For the given entropy, the density is some known function

$$\rho=f(h). \tag{99}$$

For the special case of a perfect gas $f(h)$ is simply a power of h. Since the state of the fluid is completely determined in terms of ϕ by Eqs. (97), (98), and (99), ϕ serves as the single primary variable Q that defines the flow. The conservation of

mass, which has not been used so far, then serves as the single conservation law that determines ϕ. We thus have $U=\rho$, $P=0$ in Eqs. (1) or (13), with $\mathbf{G}=0$ in Eq. (2). Both $\mathbf{F}$ and U are now functions of $\nabla\phi$.

There is a fundamental difference in the use of the potential as a primary variable, since only its gradient has physical significance. This can be seen by considering a very simple solution of the potential equation, namely uniform flow with velocity $\mathbf{u}_\infty$. The corresponding potential solution is

$$\phi = \mathbf{u}_\infty \cdot \mathbf{r}. \tag{100}$$

One cannot specify such a flow numerically without defining precisely the locations of the position vectors $\mathbf{r}$ at which the potential ϕ is discretized. While this is an obvious statement from a finite-difference viewpoint, in the finite-volume methods considered up to now the variables associated with a cell were not precisely localized. There is an important consequence in the way gradients are calculated. Applying Eq. (17) to Eq. (100) one obtains

$$\nabla\phi = \mathbf{u}_\infty \cdot (\nabla\xi\mathbf{r}_\xi + \nabla\eta\mathbf{r}_\eta + \nabla\zeta\mathbf{r}_\zeta). \tag{101}$$

The terms inside the parentheses represent the identity tensor analytically. Numerically, terms such as $\mathbf{r}_\xi$ are approximated the way ϕ_ξ is treated, while the gradients of the coordinates are obtained from Eqs. (14), (15), and (18) by approximating $\mathbf{r}_\xi$, etc. in some manner. In order to obtain the identity tensor numerically and produce the uniform velocity, the two difference approximations must be the same. This result was first obtained in [38]. It also follows from Eq. (98) that for a moving grid $\mathbf{r}_\tau$ must be differenced the same way that ϕ_τ is treated. In some algorithms, the velocity and density may be calculated at diferent points, therefore employing different difference approximations for the derivatives of ϕ. The corresponding derivatives of $\mathbf{r}$ used to calculate the gradients of the coordinates must therefore also be different.

From the above discussion it follows that for a finite-volume method, in order to preserve a uniform flow, ϕ must be defined at precise locations and the same approximations must be used for the derivatives of ϕ and the corresponding $\mathbf{r}$ in calculating $\nabla\phi$. In this respect the finite-volume method for potential flow has some of the trappings of a finite-difference method. A clear distinction can still be made in the way the cell geometry is handled. If the potentials are defined at cell centers, the cell vertices must be defined and used to calculate areas and volumes in a finite-volume method. In a finite-difference method, the position vectors at the cell centers are differenced in the same manner to calculate both the gradients and the geometric quantities appearing in Eq. (20).

For steady-state algorithms, the areas of the cell faces are the only relevant geometric quantities. Two such algorithms are the finite-volume method of Jameson and Caughey [39, 40] and the implicit algorithm of Holst [41], as extended by Flores *et al.* [38], and Thomas and Holst [42, 43]. The second algorithm is the basis of the 2-dimensional code TAIR and the 3-dimensional code TWING, both

considered finite-difference codes. But according to the definitions given above, the finite-volume and finite-difference labels should actually be *reversed.*

In both methods the conservation law is applied to secondary cells whose vertices are obtained as vectorial averages of the primary grid points at which ϕ is defined. In the method of Jameson and Caughey, all derivatives such as ϕ_ξ and $\mathbf{r}_\xi$ are obtained at the secondary grid points by centered box differencing and are then used to calculate fluxes such as $\hat{F}^\xi$ at these points. A numerical flux such as $\hat{F}^\xi_{i+1/2,j,k}$ in Eq. (54) is then obtained as the average of the values of $\hat{F}^\xi$ at those secondary grid points that are the vertices of the $i+\frac{1}{2}$, j, k face. These fluxes are further modified by adding recoupling terms to undo the effects of odd–even decoupling and explicit artificial viscosity terms to stabilize the calculation in supersonic regions. The above procedure constitutes a finite-difference method according to our definition. As is the case for the Euler equations, the area condition (6) is satisfied for 2-dimensional flow but is violated for 3-dimensional flow. In the latter case the box differencing applied to $\mathbf{r}$ is equivalent to a secondary grid with piecewise straight connections, and each face is the sum of four piecewise facets. The averaging of the fluxes at the four vertices does not correctly sum the areas of the four facets for a uniform flow. As discussed in [40], numerical errors for a uniform free stream in three dimensions are removed by subtracting free-stream fluxes from the basic equation.

In the TWING code derivatives of ϕ and $\mathbf{r}$ are obtained at the centers of the secondary faces $i+\frac{1}{2}$, j, k, etc. by centered differences of known values at the primary grid points. These are then used to calculate $\mathbf{u}$ and ρ at the face centers. The surface area vectors are calculated from Eq. (60b) in terms of the known positions of the vertices. The secondary grid is therefore assumed to have straight line connections. The flux integral is then calculated from Eq. (72). Stabilization is

to be approximately aligned with expected shock surfaces. Its value at other faces is obtained by centered averages. The procedures constitutes a finite-volume method applied to secondary cells. Note that in two dimensions, the expression for the surface area vector as calculated from Eq. (64) in terms of the vertices is identical to the corresponding derivative of $\mathbf{r}$ at the face center by centered differences. In this case the distinction between the two labels disappears. This is

faces.

The above discussion makes it clear that away from boundaries there is a blurring of distinction between finite-difference and finite-volume methods for steady-state potential flow. In a finite-difference method, an auxiliary finite volume grid can be constructed, and the relevant geometric terms can be calculated from it in order to eliminate those sources of error. Conversely, in a finite-volume method it may be necessary to construct an auxiliary finite-difference grid in order to calculate gradients properly.

Moving Grids

For an unsteady flow, a grid motion can in general influence the solution of conservation laws in three different ways. It affects the convective part of the flux due to the presence of the grid velocity in Eq. (2). This is particularly true for upwind-biased approximations. The surface area vector over which the flux is acting will in general change in both magnitude and direction. Finally, if the grid motion is not rigid, the volume of the element will undergo change. In potential flow, there is also an additional dependence of ρ on the grid velocity, as shown by Eqs. (98) and (99). In the previous section we saw that in a finite-volume method the grid points are treated in a different manner to calculate geometric quantities than the way they are used to calculate gradients. Similarly, the temporal treatment of the grid points will be different in calculating the change in geometric quantities than in the calculation of grid velocities in Eqs. (2) and (98).

Grid motion relative to a fixed reference frame has been previously studied by Thomas and Lombard [3]. The effect of a non-inertial reference frame has been treated by Holmes and Tong [12] for constant rotation and an explicit integration scheme. A generalization and unification of these results is presented here. If a rotating non-inertial reference frame is utilized, one has the choice of performing calculations with the fluid velocity components defined with respect to the inertial or non-inertial frame. In the latter instance it is generally assumed that external source terms must be present due to the rotation of the non-inertial frame. We discuss both situations and demonstrate that one can perform the numerical integration without source terms, thus preserving the strong conservation-law form. For concreteness, the discretization of general two-level implicit schemes will be presented.

In the finite-volume method, the grid velocity is treated as a geometric quantity and is interpreted as the rate of displacement of a cell face. In the standard finite-difference method, the grid velocity is normally treated as a flow variable and is combined with the fluid velocity to define a transformed velocity. This gives rise to unavoidable errors in a uniform free stream. Therefore it is necessary to treat the grid velocity in a finite-volume manner to achieve a proper finite-difference method. For this reason, the finite-volume formulation will be given in some detail, and the relevant changes for the finite-difference formulation will be indicated. Note that the procedures developed in this section are also applicable to space-marching algorithms in which the grid changes in the marching direction.

Formulation of General Grid Motion

Let $\mathbf{r}^*(t)$ be the position vector of a point relative to a non-inertial reference frame. Then the corresponding vector relative to an inertial frame has the general form

$$\mathbf{r}(t) = \mathbf{r}_0(t) + \mathbf{C}(t) \cdot \mathbf{r}^*(t), \tag{102}$$

where $\mathbf{C}$ is an orthogonal rotation tensor satisfying

$$\mathbf{C} \cdot \mathbf{C}^{\mathrm{T}} = \mathbf{I}. \tag{103}$$

The absolute velocity $\mathbf{v}$ of the point is given by Eq. (3) as the sum of

$$\mathbf{v}_r = \dot{\mathbf{r}}_0 + \dot{\mathbf{C}} \cdot \mathbf{r}^* \tag{104}$$

and

$$\mathbf{v}_c = \mathbf{C} \cdot \dot{\mathbf{r}}^*. \tag{105}$$

Here $\dot{x}$ indicates differentiation of x with respect to time for any quantity x. The velocity $\mathbf{v}_c$ may be due to the motion of a prescribed boundary surface or the use of a flow-adaptive grid. The latter may result from the motion of a free surface or the changes in some flow gradients. In the most general situation it could depend on all three.

According to the finite-volume philosophy, the geometric effects due to the grid motion are treated separately from the changes in the physical variables. Thus for a cell face with surface area vector $\mathbf{S}(t)$ we define

$$\delta V \equiv \int_{t_1}^{t_2} \int_{\mathbf{S}(t)} \mathbf{n} \cdot \mathbf{v} \, dS \, dt \tag{106}$$

to be the volume swept out by the face during the time interval Δt. δV_r and δV_c are similarly defined in terms of $\mathbf{v}_r$ and $\mathbf{v}_c$. Only the sum of the δV_c for all the cell faces contribute to the change in cell volume. The time-averaged surface area vector for the cell face is defined as

$$\bar{\mathbf{S}} = \bar{S}\bar{\mathbf{n}} = \frac{1}{\Delta t} \int_{t_1}^{t_2} \int_{\mathbf{S}(t)} \mathbf{n} \, dS \, dt, \tag{107}$$

and the time-averaged normal component of the velocity of the cell face is then

$$\bar{v}_n = \delta V / (\bar{S} \, \Delta t). \tag{108}$$

It will be convenient to express certain absolute directed vector quantities in the non-inertial frame. We thus define

$$\mathbf{u}^* = \mathbf{C}^{\mathrm{T}} \cdot \mathbf{u}, \qquad \mathbf{v}^* = \mathbf{C}^{\mathrm{T}} \cdot \mathbf{v}, \qquad \mathbf{n}^* = \mathbf{C}^{\mathrm{T}} \cdot \mathbf{n}. \tag{109}$$

Note that $\mathbf{u}^*$ and $\mathbf{v}^*$ are *not* velocity vectors relative to the non-inertial frame. Let

$$\mathbf{B}^* = \mathbf{C}^{\mathrm{T}} \cdot \dot{\mathbf{C}} \tag{110}$$

be the antisymmetric angular velocity tensor whose components form the corresponding angular velocity vector $\boldsymbol{\Omega}^*$, where

$$\mathbf{B}^* \cdot \mathbf{r}^* = \boldsymbol{\Omega}^* \times \mathbf{r}^*. \tag{111}$$

If we further let

$$\mathbf{v}_0^* = \mathbf{C}^{\mathrm{T}} \cdot \dot{\mathbf{r}}_0, \tag{112}$$

then Eq. (104) can be rewritten in the non-inertial frame as

$$\mathbf{v}_r^* = \mathbf{v}_0^* + \boldsymbol{\Omega}^* \times \mathbf{r}^*. \tag{113}$$

Discretization with Velocity Expressed in Inertial Frame

Assume that the fluid state is given at time n. In general, the position vectors $\mathbf{r}^*$ of the grid points, as well as the quantities $\mathbf{r}_0$ and $\mathbf{C}$ defining the orientation of a non-inertial reference frame, will be assumed known at times n and $n+1$. Thus the grid is assumed to be updated explicitly, even if the flow variables are updated implicitly. Unless stated otherwise, we adopt the notation

$$\Delta x = x^{n+1} - x^n \tag{114}$$

and

$$\bar{x} = \tfrac{1}{2}(x^n + x^{n+1}) \tag{115}$$

for any quantity x. The spatial indices i, j, k are omitted for brevity in this section.

In applying the finite volume method to Eq. (1), the difference in volume integrals on the left-hand side can be written as

$$\Delta(UV) = V^{n+1}\,\Delta U + U^n\,\Delta V. \tag{116}$$

In evaluating the time integral of the average flux over a face, all geometrically defined quantities are assumed held constant at their time-averaged values. The flux term can then be approximated as

$$[(1-\theta)\,F_n^n + \theta F_n^{n+1}]\,\bar{S}\,\Delta t, \tag{117}$$

where the quantities $\bar{\mathbf{n}}$ and $\bar{v}_n$ defined by Eqs. (107) and (108) are used in evaluating $F_n = \mathbf{n} \cdot \mathbf{F}$ at both time levels,. These same quantities are also used in evaluating the flux Jacobian A matrix when time linearization is used.

It is simpler to calculate the geometric quantities in the non-inertial reference frame. From the known position vectors of the cell vertices, the surface area vectors $\mathbf{S}^*$, area moments $\mathbf{M}^*$, and cell volumes V can be obtained from Eqs. (60) through (63) at times n and $n+1$, and their time-averaged values calculated from Eq. (115). ($\bar{V}$ is required if a production term is present in Eq. (1).) The conservation of volume condition (9) can be satisfied by calculating δV_c for each face exactly from the known positions of the four vertices at times n and $n+1$. A simpler method is to obtain an approximate displacement $\delta\mathbf{r}^*$ as the average of the $\Delta\mathbf{r}^*$ of the four vertices, and calculating δV_c from

$$\delta V_c \approx \bar{\mathbf{S}}^* \cdot \delta\mathbf{r}^*. \tag{118}$$

One must then use the sum of the δV_c of the six faces (with appropriate signs) in place of the true ΔV in Eq. (116). The simpler method should normally suffice, although second-order accurate algorithms with very large grid distortions may require the exact procedure.

If the grid is given in a non-inertial reference frame, one obtains δV_r for each face from

$$\delta V_r = (\bar{\mathbf{v}}_0^* \cdot \bar{\mathbf{S}}^* + \bar{\boldsymbol{\Omega}}^* \cdot \bar{\mathbf{M}}^*)\, \Delta t. \tag{119}$$

Since the $\bar{\mathbf{S}}^*$ and $\bar{\mathbf{M}}^*$ satisfy Eqs. (6) and (8) when summed over all the faces, the δV_r will sum to zero, as required by rigid body rotation. The angular velocity $\bar{\boldsymbol{\Omega}}^*$ is obtained from the components of $\bar{\mathbf{B}}^*$ calculated as

$$\bar{\mathbf{B}}^* = \frac{1}{\Delta t}\, \bar{\mathbf{C}}^{\mathrm{T}} \cdot \Delta \mathbf{C}. \tag{120}$$

One can readily show that Eq. (120) results in an antisymmetric tensor. The translational velocity $\bar{\mathbf{v}}_0^*$ is similarly calculated as

$$\bar{\mathbf{v}}_0^* = \frac{1}{\Delta t}\, \bar{\mathbf{C}}^{\mathrm{T}} \cdot \Delta \mathbf{r}_0. \tag{121}$$

The surface area vector $\bar{\mathbf{S}}$ in the inertial frame can be calculated from

$$\bar{\mathbf{S}} = \tfrac{1}{2}[\mathbf{C}^n \cdot (\mathbf{S}^*)^n + \mathbf{C}^{n+1} \cdot (\mathbf{S}^*)^{n+1}] \tag{122}$$

or

$$\bar{\mathbf{S}} = \bar{\mathbf{C}} \cdot \bar{\mathbf{S}}^*. \tag{123}$$

The second expression is simpler and differs from the first by an error of order $(\Delta t)^2$. Note that for both expression $\bar{S}$ will differ from $\bar{S}^*$ by that same order of error.

The final step is the calculation of $\bar{v}_n$ from Eq. (108), where

$$\delta V = \delta V_c + \delta V_r. \tag{124}$$

Any finite-volume algorithm discussed in the previous section can now be applied, with the grid motion included in the calculation of the flux. The change in cell volume due to grid distortion manifests itself as an additional explicit term, as shown by Eq. (116).

In a finite-difference method, the positions of the cell centers are known at times n and $n+1$. Since the grid motion just affects the convection part of the flux, it is sufficient to examine the inviscid flux terms only. For central-difference approximations, the integration of Eq. (20) over a time interval results in expressions such as Eq. (80). The evaluation of geometric quantities at each grid point is done in a manner analogous to that in the finite volume method, taking into account that

conservation is effectively applied to a doubly sized cell. Condition (21) is satisfied by calculating the surface area vectors from Eq. (81) in terms of the positions of the vertices of the doubly sized face passing through the grid point. The area moment can be analogously evaluated by applying Eq. (61) to those vertices.

Since the central-difference approximations for the effective cell volumes do not define a precise volume, one must obtain an approximate δV_c from Eq. (118), with $\delta \mathbf{r}^*$ replaced simply by $\Delta \mathbf{r}^*$ at that grid point. (It is possible to calculate a volume for the doubly sized cell that is consistent with the area formula (81), using either Eq. (62) or (63). With this additional complexity, any advantages of the finite-difference discretization are lost, and it is better to go directly to the more compact

Eq. (116) is equivalent to solving Eq. (22) by central differences. The importance of using Eq. (22) was first pointed out in [3]. The effects due to a non-inertial reference frame are handled precisely as in the finite-volume case.

Discretization with Velocity Expressed in Non-inertial Frame

For many applications in which the grid is defined in a non-inertial reference frame, it is more convenient to employ velocity components referred to axes fixed in that frame. The momentum conservation law for these components requires the presence of source terms. There is an analogy with the use of curvilinear coordinates, where the momentum equations for the curvilinear velocity components introduce source terms. But these terms can be eliminated by writing the equations for the Cartesian velocity components instead. Similarly, by employing components of the absolute velocity (as expressed in the non-inertial frame), one can also eliminate the source terms.

Let the column *vectors* U^* and F_n^*, and the matrix A^* be defined in terms of $\mathbf{u}^*$, $\mathbf{v}^*$, and $\mathbf{n}^*$ given by Eq. (109). Using the rotation matrices

$$C = \begin{bmatrix} 1 & 0 & 0 \\ 0 & \mathbf{C} & 0 \\ 0 & 0 & 1 \end{bmatrix}, \qquad C^{-1} = \begin{bmatrix} 0 & 0 & 0 \\ 0 & \mathbf{C}^{\mathrm{T}} & 0 \\ 0 & 0 & 1 \end{bmatrix}, \tag{125}$$

one can write the transformations

$$U = CU^*, \qquad F_n = CF_n^*, \qquad A = CA^*C^{-1}. \tag{126}$$

In order to reproduce a uniform flow in the inertial frame using an implicit scheme, one must use an incremented quantity proportional to ΔU, where

$$\Delta U = C^{n+1}\,\Delta U^* + \Delta C U^{*n}. \tag{127}$$

This suggests defining

$$\Delta \tilde{U}^* \equiv (C^{-1})^{n+1}\,\Delta U \tag{128}$$

and

$$\tilde{B}^* \equiv \frac{1}{\Delta t}\,(C^{-1})^{n+1}\,\Delta C = \begin{bmatrix} 0 & 0 & 0 \\ 0 & \tilde{\mathbf{B}}^* & 0 \\ 0 & 0 & 0 \end{bmatrix}, \tag{129}$$

where

$$\tilde{\mathbf{B}}^* = \frac{1}{\Delta t}\,(\mathbf{C}^{\mathrm{T}})^{n+1} \cdot \Delta \mathbf{C}. \tag{130}$$

Note that $\tilde{\mathbf{B}}^*$ differs from $\bar{\mathbf{B}}^*$ by a term of order (Δt) and is therefore not anti-symmetric. Equation (127) can now be rewritten as

$$\Delta U^* = \Delta \tilde{U}^* - \tilde{B}^* U^{*n}\,\Delta t. \tag{131}$$

The second term is only present in the momentum equation, where it represents a numerical Coriolis correction.

Before writing the implicit equation for $\Delta \tilde{U}^*$, we define the tensor

$$\tilde{\mathbf{I}} \equiv (\mathbf{C}^{\mathrm{T}})^{n+1} \cdot \mathbf{C}^n = \mathbf{I} - \tilde{\mathbf{B}}^*\,\Delta t, \tag{132}$$

and the corresponding matrix operator

$$\tilde{I} \equiv (C^{-1})^{n+1}\,C^n = \begin{bmatrix} 1 & 0 & 0 \\ 0 & \tilde{\mathbf{I}} & 0 \\ 0 & 0 & 1 \end{bmatrix}. \tag{133}$$

Note that they differ from the identity tensor and unit matrix, respectively, by terms of order (Δt). Premultiplying Eq. (116) by $(C^{-1})^{n+1}$, we obtain for the difference in volume integrals the expression

$$V^{n+1}\,\Delta \tilde{U}^* + \tilde{I} U^{*n}\,\Delta V. \tag{134}$$

The corresponding flux integral can be written in the time linearized form as

$$(\tilde{I} F_n^* + \theta A^{*n}\,\Delta \tilde{U}^*)\,\bar{S}^*\,\Delta t. \tag{135}$$

Equations (134) and (135) define an implicit algorithm to calculate $\Delta \tilde{U}^*$. This is then corrected by the Coriolis term using Eq. (131). The scheme is fully conservative and preserves a uniform free stream. Note that in order to achieve the strong conservation-law form it is necessary to use the dot product of the explicit term in the momentum equation with $\tilde{\mathbf{I}}$ and to use the proper numerical representation of the Coriolis term.

The fluid velocity vector relative to the non-inertial frame is given by

$$\mathbf{u}^{*\prime} = \mathbf{u}^* - \mathbf{v}^*. \tag{136}$$

In order to calculate it one requires $\mathbf{v}^*$ at cell centers at times n and $n+1$. The positions of the cell centers are given for a finite-difference method. For the finite-volume method one must define the location of the cell center when the non-inertial frame underdoes rotation. This situation is similar to the one discussed previously for potential flow. In addition, in order to achieve second order accuracy in time, one must know $\mathbf{r}_0$, $\mathbf{C}$, and $\mathbf{r}^*$ for each grid point at three time levels. Thus, using Eq. (136), one can treat the relative motion in an arbitrary non-inertial reference frame in a completely conservative way.

Treatment of Boundaries

The treatment of flow region boundaries depends on whether conservation is applied to cells defined by the primary or secondary grid. These will be referred to as finite-volume and finite-difference grids, respectively, even though the finite-volume and finite-difference *methods* can be applied to grids of the other family. At open boundaries, and also for upwind-biased approximations, the proper treatment of boundaries is based on characteristics considerations. Due to the 1-dimensional nature of this procedure, accurate treatment of solid wall boundaries normally employs methods that use the basic equations directly. These can be conveniently divided into two main classes. In the first class, the unknown variables on the wall are integrated together with those at interior points by an appropriate application of the conservation laws and boundary conditions. In the second class, the unknown boundary quantities needed to calculate flux terms at interior points are obtained using extrapolation, reflection principles, or some auxiliary equation. We will show how the conservation laws can also be utilized in this second approach. Both approaches will be discussed for finite-difference and finite-volume grids. Note that questions of stability and programming efficiency, although both very important, are beyond the scope of this paper. The type of grid also plays an important role at zonal boundaries and in the treatment of grid singularities. These topics are also treated in this section. Only stationary grids will be considered for simplicity.

Wall Boundary Conditions for Finite-Difference Grid

Let the wall be a constant ζ surface with index $k = 1$. Associated with the boundary point $i, j, 1$ is a secondary grid half-cell whose center is designated as the point $i, j, \frac{5}{4}$, as shown in Fig. 2. Since the points $\mathbf{r}_{i,j,0}$ do not exist, the finite difference

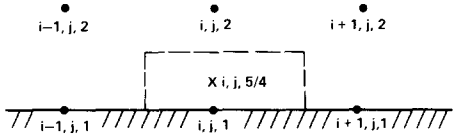

FIG. 2. Boundary half-cell for finite-difference grid.

expressions for $\mathbf{S}^{\xi}$ and V previously derived for interior points are not valid at the points $i, j, 1$. These quantities are required to calculate transport terms for points $i, j, 2$ and $i, j, 1$, as well as the geometry of the boundary half-cells. The simplest way to modify the interior formulas is to replace $\mathbf{r}_{i,j,0}$ by $\mathbf{r}_{i,j,1}$, and multiply the final result by 2. As an example, formula (81) becomes

$$\mathbf{S}^{\xi}_{i,j,1} = \tfrac{1}{4}(\mathbf{r}_{i,j+1,2} - \mathbf{r}_{i,j-1,1}) \times (\mathbf{r}_{i,j-1,2} - \mathbf{r}_{i,j+1,i}). \tag{137}$$

The use of these first-order instead of second-order accurate one-sided expressions is actually preferable for two reasons. It prevents possible unphysical answers (e.g., negative volumes) for grids with spacing discontinuities. It is also necessary in order to satisfy Eq. (6) for the doubly sized half-cell associated with the boundary point. When calculating transport terms at point $i, j, 1$ using Eqs. (17) and (18), one should use

$$(Q_{\zeta})_{i,j,1} = (Q_{i,j,2} - Q_{i,j,1})/\Delta\zeta \tag{138}$$

for consistency. Therefore the point $i, j, 2$ should be chosen close enough to the boundary to be in the linear range of the variation of Q when transport terms are important.

Extending the work of Thomas [44], we apply Eqs. (20) and (54) to the half-cell centered at the point $i, j, \frac{5}{4}$. Second-order accurate spatial differencing yields

$$\begin{aligned}(\hat{U}_{\tau})_{i,j,5/4} &+ 2(\hat{F}^{\zeta}_{i,j,3/2} - \hat{F}^{\zeta}_{i,j,1})/\Delta\zeta \\ &+ (\hat{F}^{\xi}_{i+1/2,j,5/4} - \hat{F}^{\xi}_{i-1/2,j,5/4})/\Delta\xi + (\hat{F}^{\eta}_{i,j+1/2,5/4} - \hat{F}^{\eta}_{i,j-1/2,5/4})/\Delta\eta = 0,\end{aligned} \tag{139}$$

where

$$\begin{aligned}\hat{U}_{i,j,5/4} &\equiv (\tfrac{3}{4}U_{i,j,1} + \tfrac{1}{4}U_{i,j,2})\, V_{i,j,1}, \\ \hat{F}^{\xi}_{i+1/2,j,5/4} &\equiv \mathbf{S}^{\xi}_{i+1/2,j,1} \cdot (\tfrac{3}{4}\mathbf{F}_{i+1/2,j,1} + \tfrac{1}{4}\mathbf{F}_{i+1/2,j,2}), \qquad \text{etc.}\end{aligned} \tag{140}$$

Note that a partial finite-volume approximation is employed. Thus we use $V_{i,j,1}$ and $\mathbf{S}^{\xi}_{i+1/2,j,1}$ (instead of their values at $k = \frac{5}{4}$), since these have already been defined so as to satisfy the geometric conditions.

We can eliminate $U_{i,j,2}$ using the conervative difference approximation at point $i, j, 2$. Introducing

$$\beta \equiv V_{i,j,1}/V_{i,j,2}, \tag{141}$$

we obtain for the second-order accurate conservative spatial differencing of Eq. (20) at point $i, j, 1$ the relation

$$\begin{aligned}(\hat{U}_{\tau})_{i,j,1} &+ \tfrac{1}{3}[-\beta\hat{F}^{\zeta}_{i,j,5/2} + (8+\beta)\,\hat{F}^{\zeta}_{i,j,3/2} - 8\hat{F}^{\zeta}_{i,j,1}]/\Delta\zeta \\ &+ (\tilde{F}^{\xi}_{i+1/2,j,1} - \tilde{F}^{\xi}_{i-1/2,j,1})/\Delta\xi + (\tilde{F}^{\eta}_{i,j+1/2,1} - \tilde{F}^{\eta}_{i,j-1/2,1})/\Delta\eta = 0,\end{aligned} \tag{142}$$

where

$$\tilde{F}^{\xi}_{i+1/2,j,1} \equiv \hat{F}^{\xi}_{i+1/2,j,1} + \tfrac{1}{3}(\mathbf{S}^{\xi}_{i+1/2,j,1} - \beta \mathbf{S}^{\xi}_{i+1/2,j,2}) \cdot \mathbf{F}_{i+1/2,j,2}, \qquad \text{etc.} \tag{143}$$

An important special case of Eq. (142) results from the impermeable solid wall condition

$$(\mathbf{S}^{\zeta} \cdot \mathbf{m})_{i,j,1} = 0, \tag{144}$$

valid for all flows. By combining Eq. (144) with the dot product of $\mathbf{S}^{\zeta}_{i,j,1}$ and the second component of Eq. (142), one obtains a time-independent relation expressing the conservation of normal momentum at the boundary point.

Consider first the solution of the Navier–Stokes equations for a perfect gas. The no-slip condition

$$\mathbf{m}_{i,j,1} = 0 \tag{145}$$

also results in

$$p_{i,j,1} = \kappa e_{,j,1}. \tag{146}$$

If the wall temperature is prescribed and ε_{ω} is the wall specific internal energy, then we also have the condition

$$e_{i,j,1} = \varepsilon_{w} \rho_{i,j,1}. \tag{147}$$

Thus there is only one unknown variable on the wall.

For the first class of methods, Thomas [44] suggests using the continuity equation, since the boundary conditions supplant the momentum and energy conservation laws. The first component Eq. (139) or (142) would thus be the missing equation to use in an implicit algorithm. Due to the presence of $U_{i,j,2}$ in Eq. (139), it is perhaps more appropriate to use Eq. (142), since the boundary conditions only specify the time derivatives of $U_{i,j,1}$. Actually, the wall temperature condition only relates $e_{i,j,1}$ to $\rho_{i,j,1}$ through Eq. (147), so that one could integrate the energy equation instead. Whichever equation is chosen, conservation for the remaining conservative variables will not be precisely satisfied for the boundary half-cell. Therefore some interior numerical flux terms will not be precisely cancelled, and conservation of some variables for the entire flow region will be violated in an integral sense.

As pointed out by Mehta [45] *any* independent relation can be used to integrate $U_{i,j,1}$ with time. The time-differenced form of the normal momentum equation obtained from the second component of Eq. (142) provides such a relation for the pressure. This can then be used instead of the energy equation, in view of Eq. (146). The use of the time derivative of a conservation law, as opposed to its direct employment when solving the continuity or energy equation, can have important implications in the implementation of a factored implicit algorithm. This is discussed further below.

For the second class of methods, the pressure is the only unknown wall quantity needed to calculate flux terms when applying the conservation laws at interior points $i, j, 2$. The time-independent conservative normal momentum equation at the point $i, j, 1$ provides a relationship between the wall pressures and quantities at interior points. In implicit algorithms both the direct and time-differenced forms of this relationship are required. In this respect the second method has aspects of both versions of the first method.

The practical implementation of all of these approaches could require further approximations which decrease the spatial or temporal accuracy of the algorithm at the boundary and may involve a restriction to orthogonal grids. A factored, implicit, central-differenced implementation of Eq. (139) can only be first-order accurate in time due to the presence of $U_{i,j,2}$. Flux terms such as $\mathbf{F}_{i+1/2,j,2}$ must be treated explicitly, thus again reducing the temporal accuracy to first order. One can maintain second-order accuracy in time by letting $U_{i,j,2} = U_{i,j,1}$ and $\mathbf{F}_{i+1/2,j,2} = \mathbf{F}_{i+1/2,j,1}$, but then the spatial accuracy is reduced to first order. If one used Eq. (142) instead of (139), one must still treat some flux terms explicitly and suffer a loss in temporal accuracy.

Another problem arises with the use of the time-differenced normal momentum equation for large wall curvature or severe non-orthogonality in the grid. Under those circumstances the pressure change at point $i, j, 1$ is coupled to the pressure changes at neighboring points on the boundary as well as the points $i, j, 2$ and $i, j, 3$. In an implicit updating of $U_{i,j,1}$ using this equation, *all* spatial difference operators operating on $\Delta U_{i,j,1}$ are of order one. Consequently a factored implicit algorithm is not possible. Similarly, in the second method a factored implicit treatment of the boundary flux for point $i, j, 2$ cannot be accomplished. Thus the use of the normal momentum equation in a boundary procedure for factored implicit algorithms is in principle limited to moderate wall curvature and only small non-orthogonality in the grid. Fortunately in most practical situations the grid spacing in the ζ direction is much smaller than the grid spacings along the boundary. The resulting coupling of pressure changes at points on the surface is negligible, and the above restrictions can be removed.

If the heat flux q_ω is prescribed at the wall instead of the temperature, condition (147) is replaced by

$$(k\mathbf{n} \cdot \nabla \varepsilon)_{i,j,1} = -c_v q_w, \tag{148}$$

where $k(\varepsilon)$ is the thermal conductivity and c_v is the constant specific heat at constant volume. Using Eq. (145) one has the identity

$$(\nabla \varepsilon)_{i,j,1} = \nabla(e/\rho)_{i,j,1}. \tag{149}$$

For steady-flow calculations, Hung and MacCormack [46] suggest using ∇H to evaluate the wall heat flux, since the total enthalpy H has a more linear behavior than ε. For unsteady flow, it is probably more appropriate to use $\nabla(e/\rho)$. In the first method of satisfying the boundary conditions, one now integrates both the

continuity and energy equation at point $i, j, 1$ using either Eq. (139) or (142). The alternative approach uses the time-differenced forms of the normal momentum equation and Eq. (148). These two equations are also used in the second method to calculate boundary flux terms when updating $U_{i,j,2}$.

For the solution of the Euler equations the only boundary condition is Eq. (144). In the first method of treating the boundary one would now integrate the continuity, energy, and tangential momentum equations at point $i, j, 1$ using either Eq. (139) or (142). Alternatively one could use the time-differenced form of the normal momentum equation instead of the continuity or energy equation. Since the pressure is the only unknown required to evaluate boundary flux terms, one would only need the normal momentum equation to apply the second method. However, if the wall curvature is not negligible, the expression for the pressure at point $i, j, 1$ involves the velocity and density (as well as the pressure) at neighboring points on the boundary. For example, the central difference approximation to the normal momentum equation using Eq. (142) produces the boundary terms

$$(8-\beta)(\mathbf{S}^{\zeta}\cdot\mathbf{S}^{\zeta}p)_{i,j,1} - \frac{3\,\Delta\zeta}{\Delta\xi}\left[(\mathbf{u}_{i+1,j,1}\cdot\mathbf{S}^{\zeta}_{i,j,1})(\rho\mathbf{u}\cdot\mathbf{S}^{\xi})_{i+1,j,1}+\mathbf{S}^{\zeta}_{i,j,1}\cdot(p\mathbf{S}^{\xi})_{i+1,j,1}\right]+\cdots. \tag{150}$$

There are several ways to evaluate these new unknown quantities. The simplest is to replace them by their values at the closest interior points, with an attendant loss of spatial accuracy. A more accurate procedure is extrapolation of interior values to the boundary. In the spirit of the conservation laws it is more appropriate to extrapolate ρ and $\mathbf{m}=\rho\mathbf{u}$, with the latter then projected onto the surface to satisfy Eq. (144). If the grid is highly non-orthogonal, extrapolation should probably be done in the direction normal to the surface, rather than along the ζ coordinate. A third possibility is to utilize Eq. (139) or (142) to update ρ and $\mathbf{m}$ on the surface after the interior points have been updated. This is the most rational procedure and should probably be used in the calculation of highly unsteady flows. As discussed earlier, an implicit treatment of the pressure at point $i, j, 1$ is not feasible in a factored implicit algorithm for large wall curvature or severe grid non-orthogonality.

For potential flow there is only one conservation law, and Eq. (144) gives the required boundary condition. Due to the manner in which the velocity potential ϕ on the boundary is used in solving the equation at point $i, j, 2$, one must use the first method to satisfy Eq. (144). The proper procedure is to solve Eq. (139). This is more accurate than using simple reflection principles.

Wall Boundary Conditions for Finite-Volume Grid

Let the wall be a constant ζ surface and the boundary cell be designated as $i, j, 1$. The boundary face then has the designation $i, j, \frac{1}{2}$. The position vectors

$$\mathbf{r}_{i\pm 1/2,j\pm 1/2,1}\equiv\tfrac{1}{2}(\mathbf{r}_{i\pm 1/2,j\pm 1/2,3/2}+\mathbf{r}_{i\pm 1/2,j\pm 1/2,1/2}) \tag{151}$$

and $\mathbf{r}_{i\pm 1/2, j\pm 1/2, 1/2}$ are the vertices of a boundary half-cell whose center is designated as the point, i, j, $\frac{3}{4}$, as shown in Fig. 3. In order to calculate transport terms and describe the geometry of the boundary half-cell we require the quantities $\mathbf{S}^{\zeta}_{i,j,1}$, $V_{i,j,1/2}$, and $\mathbf{S}^{\xi}_{i+1/2,j,1/2}$. $\mathbf{S}^{\zeta}_{i,j,1}$ is defined by Eq. (60) in terms of the vectors $\mathbf{r}_{i\pm 1/2, j\pm 1/2, 1}$. $V_{i,j,1/2}$, and $\mathbf{S}^{\xi}_{i+1/2,j,1/2}$ are defined as twice the corresponding expressions for the half-cell. Thus

$$\mathbf{S}^{\xi}_{i+1/2,j,1/2} = (\mathbf{r}_{i+1/2,j+1/2,1} - \mathbf{r}_{i+1/2,j-1/2,1/2}) \times (\mathbf{r}_{i+1/2,j-1/2,1} - \mathbf{r}_{i+1/2,j+1/2,1/2}). \tag{152}$$

When calculating transport terms at points i, j, 1 and i, j, $\frac{1}{2}$ using Eqs. (17) and (18), one should use

$$(Q_{\zeta})_{i,j,1} = (Q_{\zeta})_{i,j,1/2} = 2(Q_{i,j,1} - Q_{i,j,1/2})/\Delta\zeta. \tag{153}$$

Applying Eq. (5) to the boundary half-cell centered at the point i, j, $\frac{3}{4}$, one obtains the second-order accurate expression

$$\begin{aligned}(\hat{U}_{\tau})_{i,j,3/4} &+ 2[(\mathbf{S}^{\zeta}\cdot\mathbf{F})_{i,j,1} - (\mathbf{S}^{\zeta}\cdot\mathbf{F})_{i,j,1/2}] \\ &+ \hat{F}^{\xi}_{i+1/2,j,3/4} - \hat{F}^{\xi}_{i-1/2,j,3/4} + \hat{F}^{\eta}_{i,j+1/2,3/4} - \hat{F}^{\eta}_{i,j-1/2,3/4} = 0,\end{aligned} \tag{154}$$

where

$$\begin{aligned}\hat{U}_{i,j,3/4} &\equiv \tfrac{1}{2}(U_{i,j,1/2} + U_{i,j,1})\, V_{i,j,1/2}, \\ \hat{F}^{\xi}_{i+1/2,j,3/4} &\equiv \tfrac{1}{2}(\mathbf{S}^{\xi}_{i+1/2,j,1/2}\cdot(\mathbf{F}_{i+1/2,j,1/2} + \mathbf{F}_{i+1/2,j,1}), \qquad \text{etc.}\end{aligned} \tag{155}$$

Note that we use $V_{i,j,1/2}$ and $\mathbf{S}^{\xi}_{i+1/2,j,1/2}$ (instead of their values at $k = \frac{3}{4}$), since these have already been defined so as to satisfy the geometric conditions.

We can eliminate $U_{i,j,1}$ using the finite volume approximation for cell i, j, 1. Introducing

$$\beta \equiv V_{i,j,1/2}/V_{i,j,1}, \tag{156}$$

we obtain for point i, j, $\frac{1}{2}$ the second-order accurate conservative relation

$$\begin{aligned}(U_{\tau}V)_{i,j,1/2} &- \beta(\mathbf{S}^{\zeta}\cdot\mathbf{F})_{i,j,3/2} + 4(\mathbf{S}^{\zeta}\cdot\mathbf{F})_{i,j,1} - (4-\beta)(\mathbf{S}^{\zeta}\cdot\mathbf{F})_{i,j,1/2} \\ &+ \tilde{F}^{\xi}_{i+1/2,j,1/2} - \tilde{F}^{\xi}_{i-1/2,j,1/2} + \tilde{F}^{\eta}_{i,j+1/2,1/2} - \tilde{F}^{\eta}_{i,j-1/2,1/2} = 0,\end{aligned} \tag{157}$$

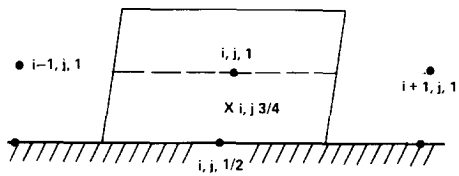

FIG. 3. Boundary half-cell for finite-volume grid.

where

$$\tilde{F}^{\xi}_{i+1/2,j,1/2} \equiv (\mathbf{S}^{\xi} \cdot \mathbf{F})_{i+1/2,j,1/2} + (\mathbf{S}^{\xi}_{i+1/2,j,1/2} - \beta \mathbf{S}^{\xi}_{i+1/2,j,1}) \cdot \mathbf{F}_{i+1/2,j,1}, \qquad \text{etc.} \tag{158}$$

The treatment of wall boundary conditions for finite-volume grids basically follows that described for finite-difference grids, with Eqs. (139) and (142) replaced by Eqs. (154) and (157), and the finite-difference boundary point $i, j, 1$ replaced by the finite-volume boundary point $i, j, \frac{1}{2}$. Note that conservation of all conservative variables for the entire flow region is automatically satisfied when a finite-volume grid is used. The purpose of introducing a boundary half-cell in this case is to relate boundary values to interior values in a conservative manner.

One can again apply the first method of treating the boundary. Note that in this case there are two boundary cells, both sharing a common boundary, that need special treatment. The boundary variable $U_{i,j,1}$ now represents an average value of U over a cell face instead of a cell-averaged quantity. The points $i, j, \frac{1}{2}$ and $i, j, 1$ are a half-cell width apart. All these factors make an implicit algorithm more involved near the boundary. Nevertheless, it is probably worth pursuing if one requires exact conservation in the integral sense *and* accurate representation of all flow variables on the boundary.

The second method of treating the boundary is obviously the natural one for a finite-volume grid. The normal momentum equation based on Eq. (157) can be utilized to various degrees of approximation for this purpose. Since the point $i, j, 1$ is closer to the boundary than the corresponding point for a finite-difference grid, one would expect these approximations to be more accurate for the finite-volume grid.

Zonal Boundaries

Another situation where the difference in the type of grid is important is the case where the boundary is a zonal boundary between two regions with completely disparate grids. The two types of grids are illustrated in Fig. 4 for 2-dimensional flow. For the finite-difference grid, the dots show the location of the grid points in one zone, and the squares the grid points in the other zone. A conservative zonal boundary procedure requires the interpolation of data between the two grids on the zonal boundary and the partitioning of flux on a flux conservation line arbitrarily chosen to lie in one of the two zones. Special handling of the fluxes is required on sides *AFE* and *BCD* of the cell straddling the zonal boundary. Excellent results have been obtained in flow calculations using this procedure by Rai [47–49]. A finite-volume grid adapts more naturally to the zonal boundary, as shown in Fig. 4b. The partitioning of the flux can now be carried out directly on the zonal boundary, leading to a conceptually simpler algorithm. Calculations using a finite-volume grid have been carried out by Rai [50] and Walters *et al.* [51].

For both types of grids, the above-mentioned zonal procedures carry out the

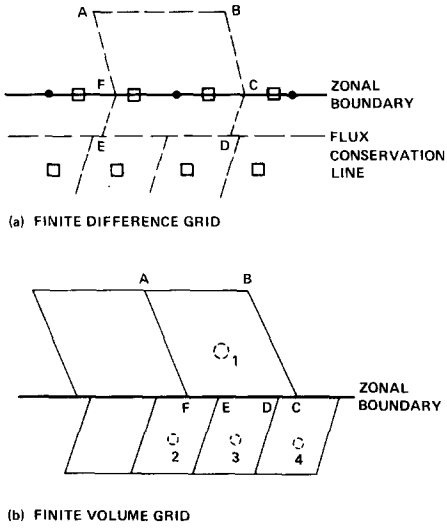

FIG. 4. Grids at zonal boundary.

partitioning of the flux in terms of the normal flux component F_n. As pointed out in [47, 51], if the flux conservation line is curved one cannot simultaneously conserve the flux and maintain a uniform free stream. However, for a finite-volume grid an alternate procedure is possible which can accomplish both objectives. For a given boundary cell one can define a separate boundary face for each cell in the [illegible] FE, ED, and DC. If a unique flux is assigned to each boundary face, then both flux conservation and free-stream maintenance is possible. For first-order accuracy, the flux across FE is calculated from U_1 and U_2; the flux across ED from U_1 and U_3; and the flux across DC from U_1 and U_4. Higher order flux calculations will involve more complex dependence on the values of U in neighboring cells. The MUSCL approach, which was also used in [51], is probably the best one in this situation. Note that boundary faces for 3-dimensional zonal boundaries will no longer be quadrilaterals in general, and expressions for a general polygonal face must be used to calculate surface area vectors. For time-accurate calculations in two and three dimensions, more general formulas for volumes of polygons and polyhedra must be used, since the boundary cells will in general not be quadrilaterals or hexahedra.

Grid Singularities

For ordered grids defined by coordinate transformation (12), grid singularities are points where the Jacobian of the transformation is either zero or unbounded. These singularities can be divided into two types. One is due to a physical corner occurring on a solid boundary that is described by a single coordinate surface. The primary grid point defining the corner is called a real singular point. The other type

occurs at singular points or curves in the interior of a flow region and also when a primary grid point on a smooth solid boundary defines a corner in a coordinate surface. Such points are termed topological singuar points.

The effect of the singular points on the numerical algorithm depends on the type of grid. For a finite-volume grid the singular points are cell vertices, and their singular nature will not affect the evaluation of geometric quantities based on straight line connections. Since the finite volume algorithms do not involve flow variables at the cell vertices, the algorithms will also not be affected by real singularities. Some modifications in the boundary procedure may be necessary for cells whose vertices include topological singular points. In either case a large loss in spatial accuracy can be expected, since the singular nature of the grid or the flow is ignored in defining average values over cell faces or cell volumes. For a finite-difference grid both U and geometric quantities must be defined for the singular points. The non-analytic behavior of U at a real singularity cannot be simply expressed. Consequently it would be difficult to account for it properly in a numerical algorithm. On the other hand, the non-analytic nature of the grid at a singular point can be expressed algebraically. This knowledge can be used to devise finite-difference algorithms near a topological singularity and to study the accuracy and stability of algorithms for both types of grids.

Previous analysis of grid singularities have been devoted to topological singularities in an interior of a flow region which occur on the boundaries of the computational space. One example is a spherical point singularity which may be introduced in calculating internal flows. A more common example is a singular curve, whose singularity is either of polar or parabolic type. Eisen [52] studied the numerical solution of the spherically symmetric diffusion equation using central differences and explicit time integration. Although his analysis was based on the nonconservative form of the equation, he treated the two types of grids that are analogous to what we term as finite-difference and finite-volume grids. A limiting form of the equation was used to obtain the differencing approximation at the singular point for the finite-difference grid. Eisen found that the finite-volume grid gave a more stable solution. An alternate stability analysis for this grid was also given by Kreiss [53]. Eriksson [54] studied the numerical solution of a 2-dimensional wave equation in the neighborhood of a parabolic singularity, using central differences. He found that the nonconservative scheme for both types of grids was unstable, but a conservative finite-volume scheme was stable. The latter had a local truncation error of order one near the singularity. A similar analysis for a polar singularity gave the same results, except that the truncation error at the singularity was now of the order of the grid spacing.

The above analyses suggest that a conservative discretization in the neighborhood of a singularity is important for stability. A finite-volume discretization based on straight line connections results in a large local error if the coordinate lines are highly curved near the singularity. A properly formulated finite-difference discretization should be capable of achieving higher local accuracy in this case. We will illustrate this by considering a topological singularity located on a smooth solid

body. The algebraic nature of the grid in the neighborhood of a corner has already been utilized to generate algebraic grids with singular corners in [55]. A similar approach will be used to obtain a Navier–Stokes central-difference algorithm near an H-type singularity in 2-dimensional flow.

Figure 5 depicts the grid in the neighborhood of the H-type singularity at $\xi = 0$ and $\eta = 0$. The part of the coordinate line $\eta = 0$ for positive ξ lies on the solid body, while the part for negative ξ lies in the flow. We assume the two parts are normal to each other at the singularity. The second method of applying boundary conditions will be used, with the wall curvature neglected. All calculations that involve quantities defined at point 0, 0 will have to be modified. The geometric quantities defined in Eqs. (14) and (15) reduce to

$$\mathbf{S}^{\xi} = \mathbf{r}_{\eta} \times \mathbf{k}, \qquad \mathbf{S}^{\eta} = \mathbf{k} \times \mathbf{r}_{\xi}, \qquad V = \mathbf{r}_{\xi} \cdot \mathbf{r}_{\eta} \times \mathbf{k} \tag{159}$$

for two dimensions, where $\mathbf{k}$ is the unit normal to the plane.

Consider first calculations for the grid point 0, 1. The grid is non-analytic between this point and the singularity. One can easily show [55] that to a good approximation

$$\mathbf{r}(0, \eta) \approx \mathbf{r}_{0,0} + (\mathbf{r}_{0,1} - \mathbf{r}_{0,0}) \sqrt{\eta/\Delta\eta} \tag{160}$$

and

$$\mathbf{S}^{\eta}(0, \eta) \approx \frac{\mathbf{S}^{\eta}_{0,1}}{\sqrt{\eta/\Delta\eta}}, \qquad \mathbf{S}^{\xi}(0, \eta) \approx \frac{\mathbf{S}^{\xi}_{0,1}}{\sqrt{\eta/\Delta\eta}}, \qquad V(0, \eta) \approx \frac{V_{0,1}}{\eta/\Delta\eta}, \tag{161}$$

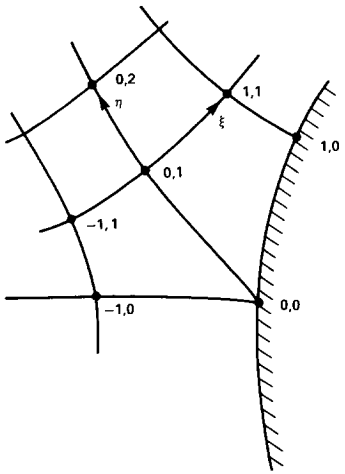

FIG. 5. Finite-difference grid near an H-type singularity.

between these two points. While $\mathbf{r}_\xi$ at point 0, 1 is calculated by the ordinary central difference formula, $\mathbf{r}_\eta$ is calculated as

$$(\mathbf{r}_\eta)_{0,1} = (\mathbf{r}_{0,3/2} - \mathbf{r}_{0,1/2})/\Delta\eta. \tag{162}$$

With $\mathbf{r}_{0,3/2}$ obtained from linear interpolation, and $\mathbf{r}_{0,1/2}$ obtained from Eq. (160), one can rewrite Eq. (162) as

$$(\mathbf{r}_\eta)_{0,1} = \frac{1}{2\,\Delta\eta}\,[\mathbf{r}_{0,2} - (\sqrt{2}-1)\,\mathbf{r}_{0,1} - (2-\sqrt{2})\,\mathbf{r}_{0,0}]. \tag{163}$$

The geometric quantities $\mathbf{S}^\xi_{0,1}$, $\mathbf{S}^\eta_{0,1}$, $V_{0,1}$, $(\nabla\xi)_{0,1}$, and $(\nabla\eta)_{0,1}$ are then obtained from Eqs. (159) and (18).

The discretization of Eq. (20) at point 0, 1 requires modification of the term

$$(\hat{F}^\eta_\eta)_{0,1} = (\hat{F}^\eta_{0,3/2} - \hat{F}^\eta_{0,1/2})/\Delta\eta. \tag{164}$$

$\hat{F}^\eta_{0,3/2}$ can be calculated by the standard methods in terms of quantities already defined. The variation of the flow variables with $\mathbf{r}$ is analytic. Therefore between the points 0, 0 and 0, 1 we can expect the inviscid part of the flux to satisfy

$$\mathbf{F}(0,\eta) \approx \mathbf{F}_{0,0} + (\mathbf{F}_{0,1} - \mathbf{F}_{0,0})\sqrt{\eta/\Delta\eta}. \tag{165}$$

Using Eqs. (161) and (165) to evaluate $\hat{F}^\eta_{0,1/2}$, we can write Eq. (164) as

$$(\hat{F}^\eta_\eta)_{0,1} = \frac{1}{2\,\Delta\eta}\,[\hat{F}^\eta_{0,2} - \hat{F}^\eta_{0,1} - (\sqrt{2}-1)\,\mathbf{S}^\eta_{0,1}\cdot\mathbf{F}_{0,0}] \tag{166}$$

for the inviscid part of the flux. The transverse component of the transport part of the flux has the same behavior as the inviscid part. In calculating the longitudinal component, we note from Eqs. (18) and (161) that $\mathbf{S}^\eta\cdot\nabla\eta$ is approximately constant between the points 0, 0 and 0, 1. Assuming that the dependence of both α and Q on η is given by Eq. (165), one obtains for the longitudinal transport flux term at 0, $\frac{1}{2}$ the relation

$$(\alpha\mathbf{S}^\eta\cdot\nabla\eta\,Q_\eta)_{0,1/2} = [\alpha_{0,1} + (\sqrt{2}-1)\,\alpha_{0,0}](\mathbf{S}^\eta\cdot\mathbf{S}^\eta/V)_{0,1}\,(Q_{0,1} - Q_{0,0})/\Delta\eta. \tag{167}$$

The calculations for the grid point -1, 0 follow the same procedure as for the point 0, 1, with the roles of η and ξ reversed. At the point 1, 0 the only quantity one requires that must be modified is

$$(\mathbf{r}_\xi)_{1,0} = \frac{1}{2\,\Delta\xi}\,[\mathbf{r}_{2,0} - (\sqrt{2}-1)\,\mathbf{r}_{1,0} - (2-\sqrt{2})\,\mathbf{r}_{0,0}]. \tag{168}$$

The only quantity required at the singular point 0, 0 is the normal gradient of Q which enters into boundary conditions. It is calculated as

$$(\mathbf{n}\cdot\nabla Q)_{0,0} = (Q_{-1,0} - Q_{0,0})/[\mathbf{r}_{-1,0} - \mathbf{r}_{0,0}]. \tag{169}$$

Note that geometric quantities at the singular point are undefined and are therefore never used. If the first method of satisfying boundary conditions is employed, one could perform calcutions for the half-polygonal cell associated with the singular point, using the concepts described above.

All the above formulas assume that the grid is sufficiently smooth. If the grid is generated algebraically, the techniques presented in [55] can be used to guarantee sufficient smoothness. In numerical grid generation schemes based on the solution of partial differential equations, the corner in the $\eta = 0$ curve will propagate into the interior using the standard procedures. One must therefore use the above concepts to modify the numerical grid generation scheme. This involves using approximations such as Eqs. (160) and (161) to derive appropriate difference approximations to partial derivatives similar to Eqs. (163) and (168).

For a finite-volume grid, second-order accuracy requires that average values are based on linear variation of the physical quantities. Geometric quantities are calculated assuming straight line connections. The finite volume method is inherently incapable of accounting for the curvature and non-analytic behavior of the grid near the singular point. Consequently, there is no simple way to modify a finite-volume algorithm near the topological singularity to obtain second-order accuracy.

Strong and Weak Conservation

The analysis in this paper has been carried out using vector notation, even though all computations are ultimately performed in terms of scalar components. This was done for two different reasons. The formulation in terms of physical vectors is more compact and gives more emphasis to the physical content of the numerical methods. Second, there are a number of different ways to obtain scalar equations from the vector equations. Most of them are motivated by a desire to keep the equations in strong conservation-law form. This terminology was coined by this author in his earlier paper devoted to the differential formulation of conser-

equations in terms of curvilinear velocity components results in additional undifferentiated terms that act like fictitious sources. This has been termed a weak conservation-law form by the author. Various methods of obtaining scalar equations in strong conservation-law form are discussed in [1]. The one most often used in practice is to write the Cartesian components of the vector conservation law. Actually, in some algorithms (e.g., [56]) it is advantageous to employ the weak conservation-law form.

In the section treating moving grids we encountered another situation that is normally thought to require the weak conservation-law form—namely the use of a non-inertial reference frame. It was shown there how the strong form can be preser-

ved by using the absolute velocity. There are two other situations that result from ignoring a space dimension in which the equations are usually expressed in weak conservation-law form. They are quasi-one-dimensional and axisymmetric flow. We now show that in a proper finite-volume formulation, the undifferentiated terms become boundary terms for the ignored direction. Thus the integral conservation law can always be satisfied for these cases.

Quasi One-Dimensional Flow

The differential formulation of quasi-one-dimensional flow results from applying the coordinate transformation $x(\xi)$ to a 1-dimensional channel whose cross-sectional area vector is

$$\mathbf{S}^{\xi} = S(x)\mathbf{i}, \tag{170}$$

where $\mathbf{i}$ is the unit vector in the x-direction. In terms of the cell volume $V = Sx_{\xi}$ and the velocity component $u = \mathbf{i} \cdot \mathbf{u}$, the continuity and energy equations for inviscid flow become

$$(\rho V)_{\tau} + (\rho u S)_{\xi} = 0 \tag{171}$$

and

$$(eV)_{\tau} + [(e+p)\, uS]_{\xi} = 0. \tag{172}$$

Since there is no flux of mass or energy at the wall, these two equations are in strong conservation-law form. The momentum equation is usually written as

$$(\rho u V)_{\tau} + [(p + \rho u^2)S]_{\xi} - pS_{\xi} = 0. \tag{173}$$

The source term pS_{ξ} results from the pressure acting on the channel walls.

In order to circumvent the weak conservation-law form, some investigators (see [57]) write the momentum equation in the quasi-conservative form

$$(\rho u V)_{\tau} + (\rho u^2 S)_{\xi} + Sp_{\xi} = 0, \tag{174}$$

in which differential terms are multiplied by geometric quantities. While this form is strictly not conservative, it satisfies the weak form of the jump conditions (11) and should possess the appropriate shock capturing capability. On the other hand, the weak form is only apparent, not real. A finite-volume discretization of the momentum conservation law for cell i gives

$$V_i(\rho u)_{\tau i} + [(p + \rho u^2)S]_{i+1/2} - [(p + \rho u^2)S]_{i-1/2} - p_{\omega i}(S_{i+1/2} - S_{i-1/2}) = 0. \tag{175}$$

Here $p_{\omega i}$ is the average pressure acting on the cell wall, while p_i is the average value of p throughout the cell. Thus the source term is actually a boundary term. The boundary condition that relates the two pressures is derived from the transverse

momentum equation. According to the quasi-one-dimensional approximation, this relation is

$$p_{\omega i} \approx p_i. \tag{176}$$

Thus the undifferentiated term only *appears* to be an interior source term when relation (176) is used as an *exact* identity to eliminate p_{wi} in Eq. (175). When one realizes that Eq. (176) is only an *approximate* relation, resulting from the approximate solution of the transverse momentum equation, one sees that the last term in Eq. (175) is really a transverse boundary term. It should be treated in an algorithm in the same manner as any other boundary term.

The proper way to discretize the equations is to apply the conservation laws to the primery grid cells, which are defined by specifying the values of $x_{i+1/2}$ and $S_{i+1/2}$ at the cell boundaries. In a finite-volume discretization, one also needs the cell volumes, which are given by

$$V_i = \tfrac{1}{2}(x_{i+1/2} - x_{i-1/2})(S_{i+1/2} + S_{i-1/2}). \tag{177}$$

Due to the quasi-one-dimensional approximation, the above relation is valid for both planar and axisymmetric flow. One can also apply the finite-volume method to secondary grid cells, with special treatment of the half-cells at the two ends of the channel.

Axisymmetric Flow

The differential formulation of axisymmetric flow differs from the 2-dimensional case primarily in the definition of geometric quantities. If $\mathbf{k}$ is the unit normal to the ξ, η plane, and y is the distance from the axis of symmetry, then one uses

$$\mathbf{r}_\zeta = \mathbf{k} \tag{178}$$

for 2-dimensional flow and

$$\mathbf{r}_\zeta = y\mathbf{k} \tag{179}$$

for axisymmetric flow in Eqs. (14) and (15). Since $\mathbf{S}^\zeta = S^\zeta \mathbf{k}$, one can also write $V = S^\zeta$ for 2-dimensional flow and $V = yS^\zeta$ for axisymmetric flow. The strong conservation-law form (20) with $\hat{P} = 0$ and the ζ derivative term absent results for both flows, except for the momentum equation. If $\mathbf{j}$ is the unit normal to the axis of symmetry in the ξ, η plane, and $v = \mathbf{j} \cdot \mathbf{u}$, then the momentum equation in the $\mathbf{j}$ direction for axisymmetric, inviscid flow is usually written as

$$(\rho v y S^\zeta)_\tau + (\hat{F}^\xi)_\xi + (\hat{F}^\eta)_\eta - pS^\zeta = 0. \tag{180}$$

The weak conservation-law form of Eq. (180) is again only apparent. The conservation law should really be applied to a wedge-shaped region of angular width $\Delta\varphi$,

where φ is the circumferential angle. Each cell extends between the two planar faces of the wedge, which act as cell boundaries in the circumferential direction. There is no convection of fluid through these boundaries, and the only contribution to the flux is the pressure in the momentum equation. The circumferential component of that equation is identically satisfied by axial symmetry. A finite-volume discretization of the radial component for cell i, j gives

$$[(\rho v V)_\tau]_{i,j} + \hat{F}^{\xi}_{i+1/2,j} - \hat{F}^{\xi}_{i-1/2,j} + \hat{F}^{\eta}_{i,j+1/2} - \hat{F}^{\eta}_{i,j-1/2} - \frac{2}{\Delta\varphi}(p_b S^{\zeta})_{i,j} \sin\frac{\Delta\varphi}{2} = 0. \tag{181}$$

The last term represents the contributions from the two circumferential boundaries, where $(p_b)_{i,j}$ is the average pressure acting on the lateral faces of cell i, j. Terms such as $\hat{F}^{\xi}_{i+1/2,j}$ are defined as in Eq. (72), while the geometric quantities are calculated from Eqs. (67)–(69). The condition of axial symmetry yields the boundary condition

$$(p_b)_{i,j} \approx p_{i,j}. \tag{182}$$

Note that this relation is not exact, since the average pressure acting on a lateral surface does not equal the pressure determined by the conservative variables averaged over the cell. Since the angular width $\Delta\varphi$ is arbitrary, we can make the further approximation

$$\frac{2}{\Delta\varphi}\sin\frac{\Delta\varphi}{2} \approx 1. \tag{183}$$

Actually, by choosing $\Delta\varphi$ small enough, one can make the error in Eq. (183) less than the round-off error in the computation, so that Eq. (183) becomes effectively an identity. We thus again find that the undifferentiated term only *appears* to be an interior source term when relations (182) and (183) are used in Eq. (181).

The proper way to discretize the equations is to apply the conservation laws to primary grid cells. The axis of symmetry then serves as a boundary of zero surface area for a row of wedged-shaped cells and consequently does not contribute to any flux calculations for those cells. One thus avoids any difficulties due to the axis singularity.

In summary, we have demonstrated for both quasi-one-dimensional and axisymmetric flow that a finite-volume discretization applied to primary grid cells enables us to preserve the strong conservation-law form. The undifferentiated terms are actually boundary terms for the flow region and should be handled in the same manner as other flow region boundary terms. While the axisymmetric case was derived for an inviscid flow, it can be readily extended to a viscous flow by including the normal viscous stress in calculating the force acting on the lateral surface.

Concluding Remarks

This survey of finite-difference and finite-volume approaches has revealed that comparisons must be made on two levels. The differences in methods (differential vs integral) leads to differences in the way geometric terms are handled. These affect questions of accuracy and programming efficiency but are not of a fundamental nature. In fact, many algorithms use a combination of both approaches. The differences in grids are more fundamental and affect many problems related to computational boundaries. The choice between the two depends on the nature of the boundary. Zonal boundaries are more naturally treated with a finite-volume grid. In order to achieve strong conservation, a finite-volume grid is also more natural for quasi-one-dimensional and axisymmetric flows. On the other hand, greater accuracy can be achieved near a topological singularity using a finite-difference grid. At a general boundary, such as a solid wall, the choice is not clear-cut. Any boundary procedure can be adapted to either type of grid. The ultimate choice will be determined by programming efficiency and stability considerations.

There is another class of discretization schemes which utilize both the finite-volume and finite-difference grids. Examples of these hybrid schemes are those of Ni [58] and Roe [59]. The conservation law is first applied to the primary cells. The changes in conservative variables are then rezoned in a conservative manner to yield the changes in the secondary cells. These are then used to update the conservative variables in the secondary cells. Since these schemes do not strictly fit into either of the classifications according to our definitions, they should properly be considered a class onto themselves.

There is a superficial resemblance between the finite-volume and finite-element methods and much semantic confusion in the literature between the two concepts. The author has addressed this question in a previous publication [60]. Conventional nodal finite-element methods define the unknowns at cell vertices of a primary grid which is usually unordered, consisting of triangles in two dimensions and tetrahedra in three dimensions. The methods do not satisfy the integral conservation laws for these cells. Thus, even though they can be formulated in a manner that provides shock capturing, they cannot be related to finite-volume methods. Several recent papers [61, 62] claim to employ the finite-element method to satisfy Eq. (1). But according to the definitions used in this paper, these methods can be classified as either finite-volume or finite-difference methods applied to an

In [61], a secondary grid with piecewise straight connections is defined by connecting the centroids of the faces of the tetrahedra to the centroids of the primary cells with straight lines. The resulting algorithm is just a finite-volume method applied to the secondary cells. The evaluation of gradients used in a higher order MUSCL scheme can be interpreted as based on the conservative definition (89) applied to the primary cells. In [62], conservation at each grid point is applied to a control volume which is the union of all the tetrahedra having this point as a vertex. Thus the conservation is effectively carried out over sets of overlapping

doubly sized cells. It is therefore appropriate to consider this a finite-difference algorithm applied to an unordered grid.

APPENDIX: Calculation of Roe-Averaged Eigenvalues

All the calculations in this Appendix are carried out for $v_n = 0$, $\gamma = 1.4$, and $\rho_L = \rho_R$. It follows from Eq. (40) that $\alpha = 0.5$.

Case 1. In this case the velocity change $\mathbf{u}_R - \mathbf{u}_L$ is assumed to be directed along the surface normal $\mathbf{n}$. Given

$$\begin{aligned} c_R &= 1.2c_L \\ u'_L &= 0.995c_L \\ u'_R &= 1.205c_L. \end{aligned} \tag{184}$$

These conditions define a transonic expansion wave. Using Eqs. (39) and (42), one determines for λ_3 the values

$$\begin{aligned} \lambda_{3L} &= -0.005c_L \\ \lambda_{3R} &= 0.005c_L \\ \bar{\lambda}_3 &= -0.005533808c_L. \end{aligned} \tag{185}$$

Note that $\bar{\lambda}_3$ does not lie between λ_{3L} and λ_{3R}.

Case 2. By increasing the normal velocity, we can convert Case 1 to

$$\begin{aligned} c_R &= 1.2c_L \\ u'_L &= 1.002c_L \\ u'_R &= 1.2102c_L. \end{aligned} \tag{186}$$

These conditions correspond to a supersonic expansion. The values of λ_3 are now

$$\begin{aligned} \lambda_{3L} &= 0.0002c_L \\ \lambda_{3R} &= 0.0102c_L \\ \bar{\lambda}_3 &= -0.000333808c_L. \end{aligned} \tag{187}$$

Note that the Roe-averaged normal velocity is now *subsonic*, even though both u'_L and u'_R are supersonic.

Case 3. This case illustrates that anomalous behavior can result just from a velocity change tangential to the surface. For concreteness we assume that $\mathbf{u}_L$, $\mathbf{u}_R$, and $\mathbf{n}$ are coplanar. Defining

$$u_t \equiv |\mathbf{u} - u_n \mathbf{n}|, \tag{188}$$

we consider the conditions

$$\begin{aligned} c_R &= c_L \\ u'_L &= 1.01 c_L \\ u'_R &= 1.02 c_L \\ u_{tR} &= u_{tL} + c_L . \end{aligned} \tag{188}$$

The normal velocity components again define a supersonic expansion. The values of λ_3 are now

$$\begin{aligned} \lambda_{3L} &= 0.01 c_L \\ \lambda_{3R} &= 0.02 c_L \\ \bar{\lambda}_3 &= -0.009697516 c_L . \end{aligned} \tag{189}$$

The Roe-averaged normal velocity for this case is also subsonic.

These three illustrative calculations indicate that conditions can exist for which the Roe-averaged eigenvalue lies outside the range determined by the states L and R.

REFERENCES

1. M. VINOKUR, *J. Comput. Phys.* **14**, 105 (1974).
2. R. W. MACCORMACK AND A. J. PAULLAY, AIAA Paper 72–154, Jan. 1972 (unpublished).
3. P. D. THOMAS AND C. K. LOMBARD, *AIAA J.* **17**, 1030 (1979).
4. R. G. HINDMAN, *AIAA J.* **20**, 1359 (1982).
5. P. L. ROE, *J. Comput. Phys.* **43**, 357 (1981).
6. R. P. REKLIS AND P. D. THOMAS, *AIAA J.* **20**, 1212 (1982).
7. J. L. STEGER AND R. F. WARMING, *J. Comput. Phys.* **40**, 263 (1981).
8. B. VAN LEER, "Flux-Vector Splitting for the Euler Equations," ICASE Report No. 82–30, Sept. 1982; in *Lecture Notes in Physics Vol. 170*, (Springer-Verlag, New York/Berlin, 1982), p. 507.
9. A. RIZZI, *AIAA J.* **20**, 1321 (1982).
10. W. KORDULLA AND M. VINOKUR, *AIAA J.* **21**, 917 (1983).
11. A. JAMESON, Department of Mechanical and Aerospace Engineering, Princeton University, Princeton, NJ, private communication (1985).
12. D. G. HOLMES AND S. S. TONG, *ASME J. Engrg. Gas Turb. Power* **107**, 258 (1985).
13. D. E. DAVIES AND D. J. SALMOND, *AIAA J.* **23**, 954 (1985).
14. S. S. TONG, Ph.D. thesis, Dept. Aero and Astro., Mass. Inst. of Tech., Cambridge, MA, 1984 (unpublished).
15. M. DRELA, M. GILES, AND W. T. THOMPKINS, JR., AIAA Paper 84-1643, June 1984 (unpublished).
16. M. GILES, M. DRELA, AND W. T. THOMPKINS, JR., in *Proceedings, AIAA 7th Computational Fluid Dynamics Conference, Cincinnati, Ohio, 1985*, p. 394.
17. A. JAMESON, W. SCHMIDT, AND E. TURKEL, AIAA Paper 81-1259, June 1981 (unpublished).
18. T. H. PULLIAM AND J. L. STEGER, AIAA Paper 78–10, Jan. 1978 (unpublished).
19. P. COLELLA, Lawrence Berkeley Laboratory Preprint LBL-17023, May 1984 (unpublished).
20. M. BORREL AND J. L. MONTAGNÉ, in *Proceedings AIAA 7th Computational Fluid Dynamics Conference, Cincinnati, Ohio, 1985*, p. 88.

21. S. K. Godunov, A. V. Zabrodin, and G. P. Prokopov, *USSR Comp. Math. Math. Phys.* **1**, 1187 (1961).
22. S. Osher and F. Solomon, *Math. Comput.* **38**, 339 (1982).
23. P. Colella, *SIAM J. Sci. Stat. Comput.* **3**, 76 (1982).
24. J. L. Montagné, *La Recherche Aérospatiale English Edition, 1984–5*, p. 21.
25. M. Pandolfi, *AIAA J.* **22**, 602 (1984).
26. J. K. Dukowicz, *J. Comput. Phys.* **61**, 119 (1985).
27. W. K. Anderson, J. L. Thomas, and B. van Leer, *AIAA J.* **24**, 1453 (1986).
28. J. E. Deese, AIAA Paper 83-0122, Jan. 1983 (unpublished).
29. D. L. Whitfield and J. M. Janus, AIAA Paper 84-1552, June 1984 (unpublished).
30. P. G. Buning and J. L. Steger, AIAA Paper 82-0971, June 1982 (unpublished).
31. L. C. Huang, *J. Comput. Phys.* **42**, 195 (1981).
32. S. R. Chakravarthy and S. Osher, AIAA Paper 85-0363, Jan. 1985 (unpublished).
33. A. Harten, *J. Comput. Phys.* **49**, 357 (1983).
34. A. Harten, *SIAM J. Num. Anal.* **21**, 1 (1984).
35. H. C. Yee and A. Harten, *AIAA J.* **25**, 266 (1987).
36. T. J. Coakley, NASA TM-85899, Feb. 1984 (unpublished).
37. S. R. Chakravarthy, K.-Y. Szema, U. C. Goldberg, J. J. Gorski, and S. Osher, AIAA Paper 85-0165, Jan. 1985 (unpublished).
38. J. Flores, T. L. Holst, D. Kwak, and D. M. Batiste, *AIAA J.* **22**, 1027 (1984).
39. A. Jameson and D. A. Caughey, in *Proceedings, AIAA 3rd Computational Fluid Dynamics Conference, Albuquerque, NM, 1977*, p. 35.
40. D. A. Caughey and A. Jameson, in *Proceedings, Symposium for the Numerical and Physical Aspects of Aerodynamic Flows, Long Beach, CA, 1981.*
41. T. L. Holst, *AIAA J.* **17**, 1038 (1979).
42. S. D. Thomas and T. L. Holst, AIAA Paper 83-0499, Jan. 1983 (unpublished).
43. S. D. Thomas and T. L. Holst, NASA TM-86716, Dec. 1985 (unpublished).
44. P. D. Thomas, in *Proceedings, AIAA 4th Computational Fluid Dynamics Conference, Williamsburg, VA, 1979*, p. 14.
45. U. Mehta, Computational Fluid Dynamics Branch, NASA Ames Research Center, Moffett Field, CA, private communication (1985).
46. C. M Hung and R. W. MacCormack, *AIAA J.* **16**, 1090 (1978).
47. M. M. Rai, *J. Comput. Phys.* **62**, 472 (1986).
48. M. M. Rai, *J. Comput. Phys.* **66**, 99 (1986).
49. M. M. Rai, *AIAA J. Prop. Power* **3**, 387 (1987).
50. M. M. Rai, Applied Computational Fluids Branch, NASA Ames Research Center, Moffett Field, CA, private communication (1986).
51. R. W. Walters, J. L. Thomas, and G. F. Switzer, AIAA Paper 86-0971, May 1986 (unpublished).
52. D. Eisen, *Numer. Math.* **10**, 397 (1967).
53. H. O. Kreiss, *Numer. Math.* **12**, 223 (1968).
54. L. E. Eriksson, The Aeronautical Research Institute of Sweden Report FFA TN 1984-10, 1984 (unpublished).
55. M. Vinokur and C. K. Lombard, in *Advances in Grid Generation, ASME Fluids Engineering Conference, Houston, TX, June 1983.*
56. T. J. Barth and J. L. Steger, AIAA Paper 85-0439, Jan. 1985 (unpublished).
57. C. K. Lombard, J. Oliger, and J. Y. Yang, AIAA Paper 82-0976, June 1982 (unpublished).
58. R. H. Ni, *AIAA J.* **20**, 1565 (1982).
59. P. L. Roe, *J. Comput. Phys.* **63**, 458 (1986).
60. M. Vinokur, NASA CR-2764, Dec. 1976 (unpublished).
61. B. Stoufflet, J. Periaux, F. Fezoui, and A. Dervieux, AIAA Paper 87-0560, Jan. 1987 (unpublished).
62. A. Jameson and T. J. Baker, AIAA Paper 87-0452, Jan. 1987 (unpublished).